APPENDIX E

SUMMARY OF RECENT INFORMATION RELEVANT TO WASTE PACKAGE AND DRIP SHIELD PROCESS MODEL

INTENTIONALLY LEFT BLANK

SUMMARY OF RECENT INFORMATION RELEVANT TO WASTE PACKAGE AND DRIP SHIELD PROCESS MODEL

1. INTRODUCTION

This white paper contains a summary of recent test results and other additional information that are relevant to the waste package degradation process model used to support the *Yucca Mountain Science and Engineering Report* (YMS&ER) (DOE 2001a) and the *Yucca Mountain Preliminary Site Suitability Evaluation* (YMPSSE) (DOE 2001b). The U.S. Department of Energy (DOE) released these two documents for public review in May and August, respectively, of this year.

The white paper focuses on the results of those laboratory tests and other additional information that became available after the waste package degradation process model was completed to support the preparation of the YMS&ER and the YMPSSE. The summary of this recent information is being used to conduct an impact review, in accordance with AP-2.14Q, *Review of Technical Products and Data*, to determine if this additional information has any impact on the technical analyses supporting the YMS&ER and the YMPSSE. The documentation of the additional information in this white paper is an interim step, and primarily used to support this impact review. This information is expected to be formally documented in subsequent Project technical reports, as appropriate.

To assist in the impact review, this white paper briefly describes the waste package degradation process model that was used to support the YMS&ER (DOE 2001a) and the YMPSSE (DOE 2001b), provides a summary of recent test results and other additional information, and discusses the potential implications of this more recent information on our understanding of the waste package degradation process model.

2. SUMMARY DESCRIPTION OF THE WASTE PACKAGE DEGRADATION PROCESS MODEL

This section provides a brief description of the component process models for waste package and drip shield degradation that were used to support the YMS&ER (DOE 2001a) and the YMPSSE (DOE 2001b). Details of the process models are given in the *Waste Package Degradation Process Model Report* (CRWMS M&O 2000a) and supporting analysis/model reports (AMRs). Reference to these documents, as appropriate, is made in the discussions that follow.

The degradation processes evaluated for the drip shield and waste package for the TSPA-SR (CRWMS M&O 2000b) include general and localized corrosion under humid-air and aqueous conditions, stress corrosion cracking, and hydrogen-induced cracking. Also considered in the TSPA-SR analysis were the effects of microbiologically influenced corrosion, aging of the waste package outer barrier, and manufacturing flaws on stress corrosion cracking of the waste package outer barrier. The WAPDEG model was used to evaluate the combined effects of the various degradation modes and to estimate the range of lifetimes of the drip shields and the waste packages, including an evaluation of uncertainties.

Thermal Aging—The long-term aging of Alloy 22 at elevated temperatures may cause the precipitation of tetrahedrally close-packed phases and/or long-range ordering which affect the corrosion resistance of the metal. The effects of tetrahedrally close-packed phase precipitation

and long-range ordering on corrosion of Alloy 22 have been investigated with electrochemical techniques, and the effect is accounted for with a general corrosion rate enhancement factor. Based on measured data, the enhancement factor is assumed to be given by a uniform distribution with an upper bound of 2.5 and a lower bound of 1 and is applied only to the closure weld region of the waste package outer barrier.

General Corrosion—General corrosion is the relatively uniform thinning of materials without significant localized corrosion. Dry oxidation (dry-air corrosion) occurs at a relative humidity below the threshold for humid-air corrosion. Dry-air corrosion is expected to have no significant impact on waste package and drip shield performance.

Humid-air corrosion is defined as corrosion in the absence of dripping water. Aqueous-phase corrosion requires the presence of dripping water. In the TSPA-SR, carbonate-base water, which has characteristics of J-13 well water, was considered the most likely to contact the drip shield and waste package. The threshold relative humidity for humid-air and aqueous-phase corrosion is based on the deliquescence point of sodium nitrate salt.

The distributions of general corrosion rates for Alloy 22 and Titanium Grade 7 used in the TSPA-SR model are based upon weight-loss data from the Long-Term Corrosion Test Facility collected after a two-year exposure period. The corrosion data for Alloy 22 and Titanium Grade 7 indicate that the general corrosion rates for humid-air and aqueous-phase corrosion are about the same. The data also show little sensitivity to exposure temperature for the water chemistry and temperature ranges considered in the test program. The calculated general corrosion rates were corrected for the effects of silica scale deposits on the sample coupons, which may have added to the post-exposure weight. Based on an estimated amount of deposit, the general corrosion rate from the weight-loss measurements was increased by as much as 0.063 μm/yr. The general corrosion rate distributions for Alloy 22 and Titanium Grade 7 include substantial uncertainties. Most of the uncertainties result from the uncertainties in the weight-loss measurements due to the extremely low corrosion rates of the materials in the test environments.

Localized Corrosion—The localized corrosion model for waste package materials assumes that localized attack occurs if the open circuit corrosion potential (E_{corr}) exceeds the threshold (critical) potential for breakdown of the passive film (E_{crit}). The correlation is based upon standard cyclic polarization measurements in a variety of test solution media covering a broad range of temperatures. Because the threshold potentials on the waste package and drip shield surfaces were not exceeded, both the waste package and drip shield are never subject to localized corrosion.

Microbiologically Influenced Corrosion—It has been observed that Titanium Grade 7 and Alloy 22 are relatively resistant to microbiologically influenced corrosion. Furthermore, microbial growth in the repository will be limited by the availability of nutrients. The TSPA-SR analysis assumes that when the relative humidity at the surface of the waste package and drip shield is greater than a threshold value (i.e., 90 percent relative humidity), microbiologically influenced corrosion can occur on Alloy 22. The TSPA-SR assumes that Titanium Grade 7 is not subject to microbiologically influenced corrosion. The effect of microbiologically influenced corrosion on Alloy 22 is modeled with a general corrosion rate enhancement factor. This factor,

based on the ratio of measured corrosion current densities for inoculated and abiotic samples, is determined to be in the range of 1 to 2.

Stress Corrosion Cracking—Stress corrosion cracking (SCC) is a potential degradation mode that can result in penetration of the waste package outer barrier (Alloy 22). SCC of materials may occur when an appropriate combination of material susceptibility, tensile stress, and environment is present. SCC is assumed to occur only in the regions around the closure welds of the Alloy 22 outer barrier because the residual stress in this weld cannot be relieved completely. The SCC model includes two alternative models, one based on the slip-dissolution mechanism at the crack tip for crack initiation and propagation, and another based on the threshold stress intensity factor at the tip of preexisting flaws. The slip dissolution model employs a threshold stress for crack initiation. SCC is initiated if the threshold stress is exceeded on a smooth surface. The parameters for the slip dissolution model are based on data for stainless steel in the boiling water reactor industry.

While the slip dissolution model allows for crack growth at any surface defect that can generate a positive stress intensity factor, a review of the relevant SCC literature indicates that there is a threshold stress below which SCC will not initiate on a "smooth" surface. This threshold stress is estimated to be in the range of 20 to 30 percent of the yield strength based on data for stainless steels.

An effective approach to eliminate the threat of SCC, and the resultant through-wall cracking in the closure weld region, is to implement a post-weld stress mitigation process to either remove residual tensile stresses in the weld region or reduce them below threshold values for SCC initiation and growth. Mitigation processes which result in compressive stresses on the surface delay the onset of SCC. The TSPA-SR SCC model also uses data on the density, size, and the orientation of flaws as key parameters in the model.

Hydrogen-Induced Cracking—Evaluation of hydrogen-induced cracking (HIC) is based upon a threshold hydrogen concentration. The basic premise of the model is that failure will occur after the hydrogen content exceeds a certain limit, or critical value. The threshold value for Titanium Grade 7 is evaluated to be at least 1,000 μg/g. Analyses of a worst-case scenario, which assumes local concentration of hydrogen from the galvanic coupling and the contact area produced by a rock bolt falling on the drip shield, conclude that failure due to hydrogen embrittlement is unlikely.

3. SUMMARY OF RECENT TEST RESULTS AND OTHER ADDITIONAL INFORMATION

This section summarizes recent results obtained from laboratory tests and other sources that have provided information relevant to enhancing our understanding of the waste package degradation process model. The testing activities and other sources that provided this additional information are listed below and discussed in each of the sections that follow:

1. Environment on the drip shield and waste package outer barrier
2. Aging and phase stability of the waste package outer barrier
3. Passive file stability

4. General and localized corrosion
5. Stress corrosion cracking
6. Stress mitigation and weld stress measurement
7. Waste Package Materials Performance Peer Review.

Because of the recent nature of the information provided in this section, much of it is unpublished and, therefore, the source references have not been provided. However, this information is currently documented in the principal investigators' scientific notebooks, if applicable, in accordance with the Project's quality assurance procedure AP-SIII.1Q, *Scientific Notebooks*.

3.1 ENVIRONMENT ON THE DRIP SHIELD AND WASTE PACKAGE OUTER BARRIER

3.1.1 Deliquescence Point

Relative humidity is known to have an effect on the corrosion susceptibility of metallic materials that have hygroscopic salt deposits on their surfaces. Corrosion susceptibility occurs when the relative humidity is at or exceeds the deliquescence point of the hygroscopic salt. The deliquescence point of a salt is the lowest relative humidity where an aqueous solution of that salt is thermodynamically stable.

The deliquescence points of several pure salts over a range of temperatures are documented in *Environment on the Surfaces of the Drip Shield and Waste Package Outer Barrier* (BSC 2001b). The values range from 35 to 20 percent relative humidity for very hygroscopic salts, such as $MgCl_2$ and KF, to greater than 95 percent relative humidity for K_2SO_4. Binary salt mixtures will have a deliquescence point that is lower than that for either of the two components (e.g., Wexler and Seinfeld 1991). (The deliquescence point lowering is also true for multicomponent systems.) As an example, Wexler and Seinfeld (1991) calculated the binary phase diagram for the NH_4Cl – NH_4NO_3 system shown in Figure 1 below.

There are three deliquescence points for the NH_4Cl – NH_4NO_3 system. For pure NH_4Cl, the deliquescence point is 77.4 percent relative humidity. For pure NH_4NO_3 the deliquescence point is 59.4 percent relative humidity. The binary mixture deliquesces at 51.4 percent relative humidity with an aqueous solution composition of 0.811 mole fraction NH_4NO_3. At relative humidities above 51.4 percent relative humidity, the aqueous solution will have the same composition as the salt mixture if the relative humidity is also above the "two phase-aqueous phase" line, or "liquidous" (lines 1 and 2 in Figure 1). If the relative humidity for a given mixture is above 51.4 percent relative humidity but below the "liquidous" line, then the aqueous phase has a composition equal to that specified by the intersection of the "liquidous" line and a line parallel to the x-axis at the given relative humidity. Further, the amount of aqueous solution and dry salt is determined by a "tie line" analysis.

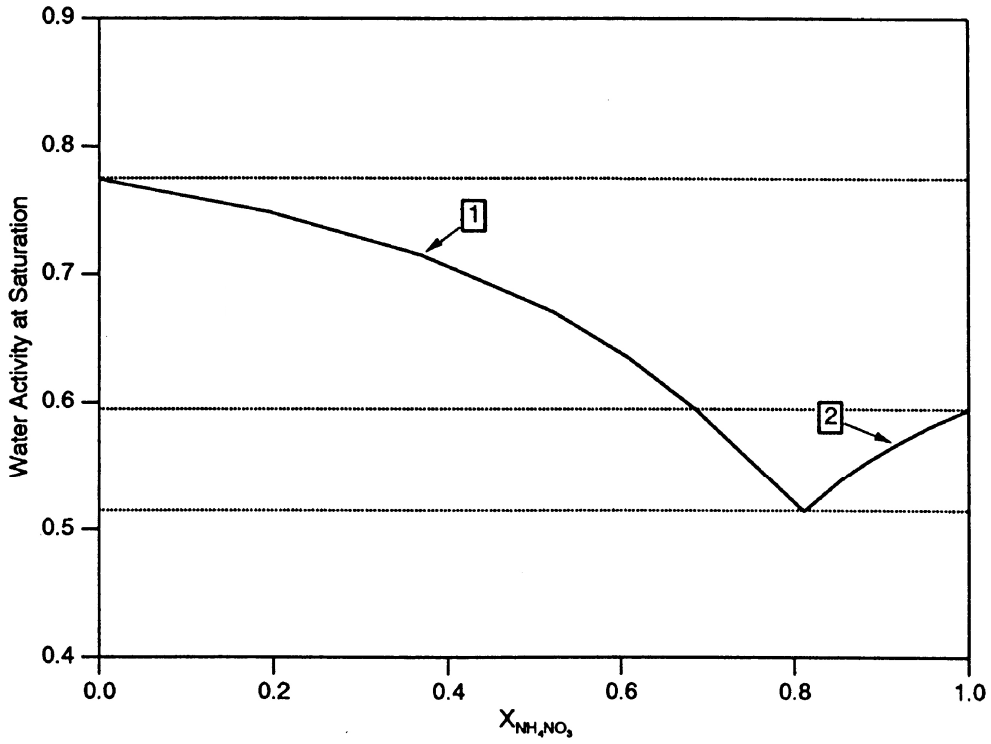

Figure 1. Water activity (or equivalently, relative humidity) at saturation of an aqueous solution of NH_4NO_3 and NH_4Cl

It is known that certain anionic species have an inhibiting effect on halide-induced localized corrosion. This inhibiting effect is a function of both temperature and the concentration of the inhibiting ion(s) relative to the halide ion. For instance, it has been shown that nitrate and sulfate have such an inhibiting effect on localized corrosion of Alloy 22 when they are present at certain concentrations relative to chloride ion content (Kehler et al. 2001). The susceptibility to localized corrosion is indicated by the decrease in the "repassivation potential" for crevice corrosion as the chloride to nitrate plus sulfate ratio increases.

The effect of a deposited salt on localized corrosion susceptibility is then a function of relative humidity. For example, if the chloride to nitrate ratio for localized corrosion susceptibility is greater than or equal to one, then the relative humidity must be greater than 68 percent for the system in Figure 1 before other factors influencing localize corrosion, such as the corrosion potential, need to be considered. This relative humidity is significantly higher than the deliquescence point of the salt mixture. Hence this solution composition dependence on relative humidity decreases the region of susceptibility to localized corrosion when compared to "turning on" susceptibility at the deliquescence point of the salt mixture. A similar type of analysis would hold for multi-component salt systems.

3.1.2 Trace Elements

Metals at trace concentrations in aqueous solutions are known to have an effect on corrosion processes affecting metallic alloys. For example, trace amounts of lead (Pb) may affect the corrosion of Alloy 600, a nickel-chromium alloy, as an oxidation-reduction couple (Byers

et al. 1997), and trace amounts of arsenic (As) are known to assist in hydrogen embrittlement of type 304 stainless steel (Hermas 1999). To assist in characterizing the extent that trace metals may affect corrosion of candidate materials, the trace metal geochemistry in ambient Yucca Mountain groundwater was evaluated with regards to generating elevated dissolved lead, arsenic, and mercury levels in the potential repository environment. The chemical composition of water that might come in contact with engineered components at Yucca Mountain is expected to be an oxidizing, neutral to alkaline brine, that evolves as fairly neutral (pH 5-8), dilute ambient groundwater interacts with the Yucca Mountain geology at elevated temperature. End-member brines are expected to be alkaline (pH 10) Na-HCO_3-CO_3 brines and/or more neutral (pH 6) Na-K-Ca-Mg-Cl-NO_3 and Na-K-Mg-Cl-SO_4-NO_3 brines.

Lead—Ambient levels of dissolved lead are at trace levels in groundwater in the vicinity of Yucca Mountain (~9 ppb, Perfect et al. 1995). In general, dissolved lead concentrations in groundwater are controlled by precipitation of lead containing minerals (e.g., carbonates and oxides in oxidized waters and sulfides in reduced waters) as well as lead adsorption onto mineral surfaces (Drever 1997). Ambient lead levels in groundwater, which would evolve into near neutral to alkaline brines, have the potential to concentrate in these brines, however concentration levels are expected to be limited to at or below the ppm level. Depending on brine pH and anion levels, lead-chloride, -carbonate and -hydroxyl complexes can either decrease or increase lead solubility.

Arsenic—A potential source of arsenic in Yucca Mountain groundwater is volcanic glass, which slowly dissolves and releases arsenic (Welch et al. 1988). The trace arsenic levels in ambient Yucca Mountain groundwater (~1 ppb, Perfect et al. 1995) have the potential to concentrate in repository brines as the groundwater evaporates because dissolved arsenic has few solubility controls in oxidizing groundwater (Hem 1992). This conclusion is supported by high dissolved arsenic concentrations measured in geothermal waters and in alkaline lakes, which can contain arsenic at the ppm level (Stauffer and Thompson 1984; Anderson and Bruland 1991; Maest et al. 1992; Oremland et al. 2000). It should be noted that arsenic is still a minor constituent in these waters. Sorption processes may limit dissolved arsenic concentrations from pH 4-7 in dilute groundwater (Hingston et al. 1971; Anderson et al. 1976; Frost and Griffin 1977; Pierce and Moore 1980; van der Hoek et al. 1994; Wilkie and Hering 1996). However arsenic sorption will be diminished in more concentrated brines, containing high dissolved silica or phosphate that compete for surface sorption (Hingston et al. 1971; Swedlund and Webster 1998). It is possible for some cement minerals to remove As(V) from alkaline water above pH > 10.7 (Myneni et al. 1997).

Mercury—Ambient Yucca Mountain groundwater mercury concentrations are expected to be quite low based on the composition of other pristine groundwaters (10^{-2} to 10^{-3} ppb) (Krabbenhoft and Babiarz 1992; Zelewski et al. 2001). Similar to arsenic, mercury has few solubility controls (Hem 1992). However, the ability of mercury to concentrate in brines will be limited because it is volatile and transfers to the atmosphere, especially at elevated temperatures anticipated in the potential repository environment. Although mercury does sorb to clay minerals, its role in concentrated brines will be diminished because mercury forms chloride complexes that do not sorb effectively to mineral surfaces (MacNaughton and James 1974; Barrow and Cox 1992; Tiffreau and Trocellier 1998).

3.2 AGING AND PHASE STABILITY OF THE WASTE PACKAGE OUTER BARRIER

Measurements have been made to quantify the amount of grain boundary precipitation of tetrahedrally close-packed phases that occurs in aged Alloy 22 (Scientific Notebook #LLNL-SCI-434-VI). Alloy 22 samples were aged at temperatures between 427° and 760°C (801° and 1,400°F) for times up to 40,000 hours. The samples were examined in the as-polished condition in a scanning electron microscope in the backscattered electron detector mode. A number of areas were examined depending on how much precipitation was present (more areas were needed for very small amounts of precipitation). In each area, the total grain boundary length and the length of grain boundary covered by tetrahedrally close-packed phases were measured. The fraction of grain boundaries covered by tetrahedrally close-packed phase precipitation was recorded as a function of time and temperature.

The time required to cover 50 percent and 85 percent of the grain boundaries is plotted in Figure 2 as a function of reciprocal temperature. This figure also shows the point corresponding to 10,000 years and 300°C (572°F). Extrapolation of the data intersects the line corresponding to 10,000 years to the left of this point. Because the horizontal axis corresponds to reciprocal temperature, this means that grain boundary precipitation can only occur in 10,000 years at temperatures much higher than 300°C (572°F). The location of the line corresponding to 15 percent coverage of the grain boundaries is estimated assuming the lines corresponding to 15 percent and 85 percent are equidistant from the 50 percent line. Thus, even the early stages of precipitation are not expected at the low temperatures expected in a repository.

3.3 PASSIVE FILM STABILITY

A thorough understanding of passive film stability is necessary to establish the performance of corrosion resistant materials such as Alloy 22 and Titanium Grade 7 for time periods in excess of 10,000 years. In addition to direct studies of these materials, knowledge of natural and industrial analogues is also used.

3.3.1 Background on Passive Film Stability

The exceptional corrosion resistance of Alloy 22 is due to the thermochemical stability of the passive film over a very broad range of potential, pH and temperature. The additions of Mo and W to this alloy tend to stabilize the passive film and prevent localized corrosion at low pH and high chloride (Farmer et al. 2000). The recognition of the importance of molybdenum as a means of stabilizing the passive film dates back to the 1980s (Farmer et al. 1988, Figure 24, p. 30) and was based upon a seminal publication by Haynes International (Asphahani 1980). Asphahani compared the resistance to localized corrosion of a series of iron-nickel-chromium alloys, each having a different concentration of molybdenum. In this series, C-276 had the best corrosion resistance, and has a composition very close to that of Alloy 22. Thus, C-276 is an industrial analogue. More recently, corroborative trends in the passive current densities have been presented for C-4, 625, C-276, C-2000 and C-22 (Alloy 22) in 1M NaCl solutions at pH~1 by Lloyd and Shoesmith at Stainless Steel World 2001. These recent data show that Alloy 22 has the lowest passive corrosion density in this family of materials and further substantiate the decision to use this material for construction of the waste package.

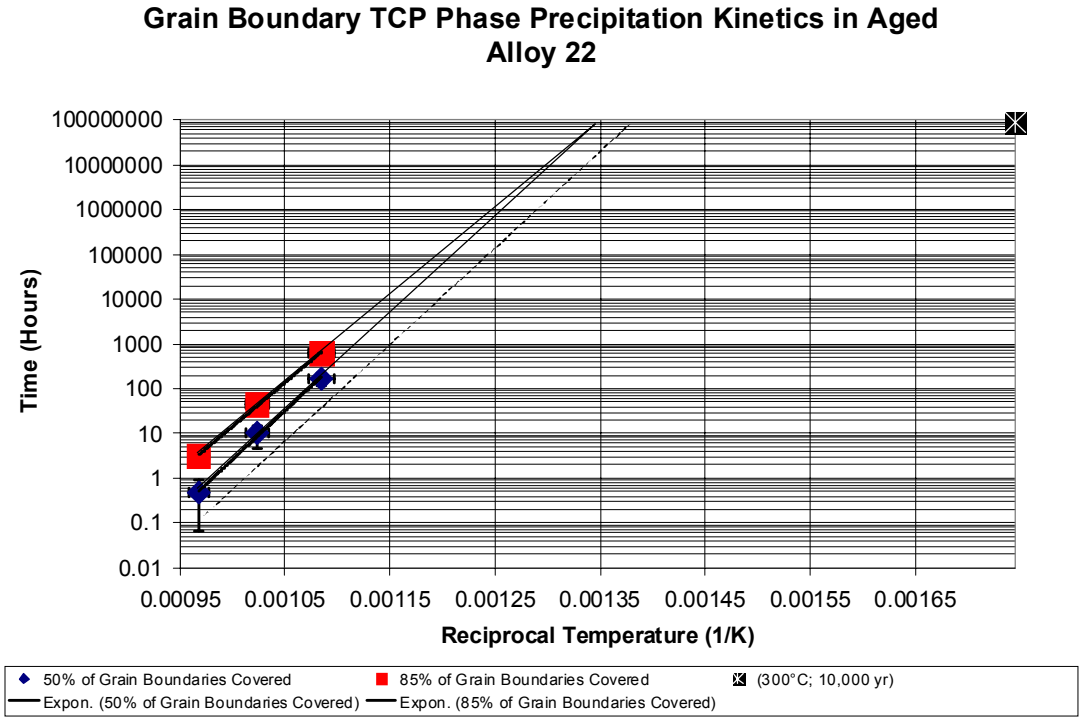

Note: The dashed line is an estimate of the position of the line that would correspond to 15 percent of the grain boundaries being covered by tetrahedrally close-packed phase precipitation.

Figure 2. The Time Required for 50 and 85 Percent of the Grain Boundaries in Alloy 22 to be Covered by Tetrahedrally Close-Packed Phase Precipitation as a Function of Reciprocal Temperature

Resistance to localized corrosion is quantified by a differential potential, the separation between the open circuit corrosion potential and the critical potential. As shown in *General Corrosion and Localized Corrosion of Waste Package Outer Barrier* (CRWMS M&O 2000c, Figures 3 and 4), the differential potentials for Alloy 22 in simulated acidic water (SAW) at pH~3 and 90°C (194°F) and in simulated saturated water (SSW) at pH~7 and 120°C (248°F) are both very large, indicating exceptional passive film stability in these hot concentrated brines. Also shown in *General Corrosion and Localized Corrosion of Waste Package Outer Barrier* (CRWMS M&O 2000c, Figures 5 and 6), Alloy 22 in simulated concentrated water (SCW) at pH~11 and 60° and 90°C (140° and 194°F) exhibits a pronounced anodic oxidation peak between 200 and 400 mV versus SCE. X-ray photoelectron spectroscopy of the passive film formed during polarization in this alkaline medium indicates that this anodic peak is probably due to the conversion of Mo(IV) to Mo(VI) within the passive film. The thermal aging of Alloy 22 for 173 hours at 700°C (1,300°F) does not appreciably change the overall appearance of the polarization curves in the aforementioned test media (CRWMS M&O 2000c, Figures 44 and 45). Saturated brines formed by evaporative concentration have sufficient buffer and inhibitor present to prevent crevice corrosion at ambient temperature (CRWMS M&O 2000c, Figure 43). Similar results have been obtained with creviced samples tested near the boiling point. No pitting, crevice corrosion, or stress corrosion cracking has yet been observed in the Long Term Corrosion Test Facility, after more than four years of testing in hot concentrated brines.

3.3.2 Natural Analogue—Stability of Metallic Josephinite (Awaruite)

Sample Description—A sample of josephinite was purchased from Harvey B. Meieran (Orme 2001). This sample is assumed to have been found in a riverbed. However, there is no information on its geological history, or more specifically, exactly how long it had been exposed to water. Josephinite is the name given to rock samples bearing the metallic minerals awaruite and possibly taenite dispersed among other nonmetallic minerals (BSC 2001a). Taenite is a face-centered cubic solid solution of iron (Fe) and nickel (Ni). Awaruite, which is more prevalent in josephinite, is an ordered phase with the stoichiometry of Ni_3Fe, but possible compositions of awaruite range from 63 to approximately 90 at percent Ni. Because the conditions under which josephinite forms become less and less reducing over time, the outer layers tend to be nonmetallic. These outer layers presumably provide protection of the inner metallic minerals over times on the order of 150 million years. In some samples, however, metallic minerals have been observed near the josephinite surface (BSC 2001a). This sample (Figure 3) was examined because it had a more metallic appearance than other samples obtained previously. It had been worn smooth, but whether this occurred naturally is not known. During this study, the nominal composition was found to be approximately 27.57 atomic percent Fe and 72.43 atomic percent Ni. During sputtering, the average Ni/Fe ratio of the rock was ~3.4 which is consistent with the composition of awaruite.

Note: The black areas are thought to be a magnesium silicate. The metallic-looking areas were the subject of this investigation.

Figure 3. Optical Image of the Josephinite Rock Used for the X-Ray Photoelectron Spectroscopy Studies

Surface Analysis—The surface layers of the sample in Figure 3 were examined using X-ray photoelectron spectroscopy at Lawrence Livermore National Laboratory (see Table 1). First, X-ray photoelectron spectroscopy was performed on the surface of the sample in the "as received" condition. Spectra were dominated by signals for carbon (~80 percent), though signals for iron and nickel were also detected (~0.5 percent). The oxidation states of iron and nickel in this surface layer are ambiguous due to the weakness of the respective signals. There was also a small signal emanating from the surface layer that is attributed to the presence of silicate. After analysis of the surface layer, depth profiling was performed using argon ion beam sputtering.

Spectra were captured as surface layers were removed by ion milling at a rate of approximately 2 nanometers per minute, with exploration of depths from 2 to 120 nanometers. A broad spectrum captured at a depth of 2 nanometers indicated that nickel was in its elemental (reduced) form. Since X-ray photoelectron spectroscopy signals from oxidized forms of nickel are distinctly different from the elemental (reduced) form, and since such signals were clearly absent at depths as great as 120 nanometers, the surface layers are believed to contain no nickel oxide. In contrast, signals for both elemental (reduced) and oxidized forms of iron were detected during depth profiling. However, it was difficult to determine whether the oxide detected was Fe_3O_4 and Fe_2O_3 since the difference in the binding energies for Fe(II) and Fe(III) are relatively small. Because the surface is rough over the lateral extent of the beam (500 μm), it should be cautioned that the spectra represent material from a range of depths. Also, magnetite (Fe_3O_4) is commonly found in josephinite.

Table 1. X-ray Photoluminescence Spectroscopy Data (in atomic percent) from the Surface of the Josephinite Sample Shown in Figure 3

Samples	Fe2p	Ni2p	F1s	O1s	C1s	Si2p
Spot 1 as received	0.5 oxide and elemental	0.1 oxide	0.2	18.7	78.5	2.0
Spot 2 as received	0.3 oxide and elemental	-- oxide	--	10.8	87.2	1.8
Spot 3 after 1 minute	3.4 oxide and elemental	12.3 elemental	--	13.7	67.9	2.6
Spot 3 after 5 minutes	5.6 oxide and elemental	16.8 elemental	--	19.5	58.2	--
Spot 3 after 25 minutes	9.9 oxide and elemental	32.6 elemental	--	23.4	34.2	--
Spot 3 after 40 minutes	10.1 oxide and elemental	37.0 elemental	--	24.4	28.5	--
Spot 3 after 60 minutes	12.0 oxide and elemental	41.6 elemental	--	22.7	23.8	--

NOTE: Spots 1 and 2 were taken from the surface of the sample. Spot 3 was taken as a function of sputtering time (or depth). All three spots were within the metallic looking regions of the sample.

Indication of High Porosity—The sample of josephinite produced significant out-gassing, making it difficult to attain sufficient vacuum to perform X-ray photoelectron spectroscopy. This out-gassing is believed to be due to high porosity of either the black surface layer, the bulk volume of the mineral, or both.

Conclusion—As previously discussed, the presence of molybdenum in the passive film of Alloy 22 is responsible for imparting exceptional corrosion resistance, especially in situations where low pH can develop. Note that occluded geometries, such as crevices and pits are especially susceptible to pH lowering due to hydrolysis reactions within the crevice, and differential aeration. Since josephinite and other natural analogues such as meteorites are primarily composed of iron and nickel, the passive films have no stabilizing elements such as molybdenum and tungsten. This has now been established through detailed investigations of the naturally occurring layers that form on at least one of these metallic minerals. Therefore, direct comparison of long-time performance of Alloy 22 to the longetivities of josephinite and

meteorites are inappropriate. The presence of a less corrosion resistant metal near the surface of minerals that have survived for over 100 million years, however, does provide confidence in the ability of Alloy 22 to remain passive under potential repository conditions.

3.3.3 Electrochemical Studies of Passive Film Stability in Brines

Corrosion Potential Indicative of Passive Film Stability—As previously discussed, both the open circuit corrosion potential and the critical potential are indicators of passive film stability. A stable passive film would be expected to have a stationary, time invariant corrosion potential in an unchanging environment. Furthermore, the difference between the corrosion and critical potentials should remain large.

Corrosion Potentials in Fresh Solutions—Additional confirmatory testing has now been done at the General Electric Corporate Research and Development Center (GECRD) to corroborate the findings at Lawrence Livermore National Laboratory. Samples of Alloy 22 and Titanium Grade 7 were polished to a 600-grit finish with standard SiC media. A standard saturated Calomel reference electrode (SCE) was used. The GECRD test solution used in these tests is described in Table 2. In essence, this solution is equivalent to 2,800× J-13 well water, and has a pH of approximately 12.2.

Table 2. Solution Used in Corrosion Tests at GECRD

10.6 g Na_2CO_3 (anhydrous)	9.7 g KCl
8.8 g NaCl	0.2 g NaF
13.6 g $NaNO_3$	1.4 g Na_2SO_4 (anhydrous)
4.1 g $Na_2SiO_3 \bullet 9H_2O$	1000 g H_2O

A steady-state open-circuit corrosion potential was established at 95°C (203°F) during the test, as shown in Figure 4. The measurements of open circuit corrosion potential for Titanium Grade 7 decreased with time, and ranged from –80 to –140 mV versus SCE. The measurements for Alloy 22 also decreased with time, and ranged from –140 to –200 mV versus SCE. The presence of salt deposits was found to increase the open circuit corrosion potential by about 20 mV.

For comparison, consider the open circuit corrosion potentials previously determined by Lawrence Livermore National Laboratory and published in the respective AMRs (CRWMS M&O 2000c; and CRWMS M&O 2000d). In the case of Alloy 22, measurements are found in *General Corrosion and Localized Corrosion of Waste Package Outer Barrier* (CRWMS M&O 2000c, Table 6). Values of the open circuit corrosion potential for Simulated Dilute Water (SDW), SCW, SAW, and SSW at 90°C (194°F) are –183, -220, -168, and –208 mV versus Ag/AgCl, respectively. These values for Alloy 22 agree with the values measured by GECRD that are shown in Figure 4 (–140 to –200 mV versus SCE, or –95 to –155 mV versus Ag/AgCl). The GECRD measurements are close to those for SDW and SAW, and are therefore considered to be corroborative.

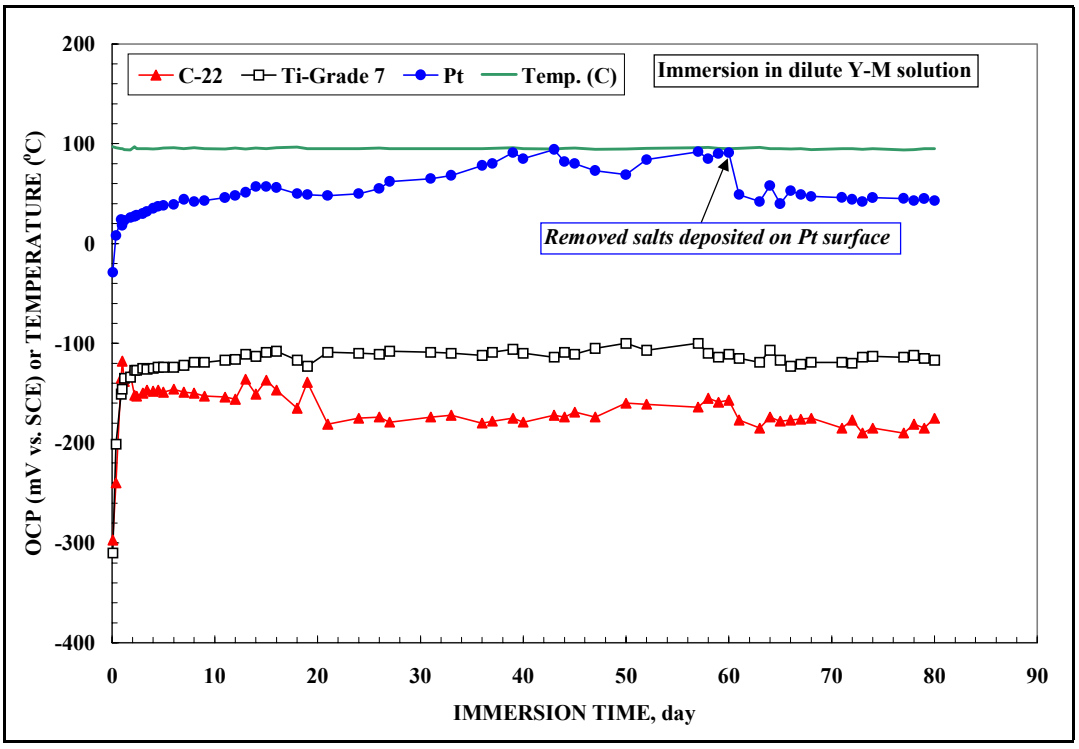

Figure 4. Open Circuit Corrosion Potential of Waste Package Materials as a Function of Immersion Time

In the case of Titanium Grade 7, measurements are found in *General Corrosion and Localized Corrosion of the Drip Shield* (CRWMS M&O 2000d, Table 4). Values of the open circuit corrosion potential for SDW, SCW, SAW, and SSW at 90°C (194°F) are –305, -480 to -516, -176 to -187, and –336 mV versus SCE, respectively. These values for Titanium Grade 7 are considered to be substantially different than the measurements by GECRD that are shown in Figure 4 (–80 to –140 mV versus SCE). It is noted, however, that the corrosion potential of titanium in Figure 4 is initially approximately –300 mV versus SCE and increases over a period of nearly two days. Since the cyclic polarization measurements, used to generate the values above, are done after a period of time on the order of a few hours, these values are considered to be consistent with those shown in Figure 4. One should also note that the GECRD measurements are still well below the critical potential for localized corrosion initiation.

Corrosion Potentials in Aged Long-Term Corrosion Test Facility Solutions—Studies of the open circuit corrosion potential at Lawrence Livermore National Laboratory have shown a dependence of the measurements on immersion time. Samples exposed for several years in the Long-Term Corrosion Test Facility exhibit higher apparent corrosion potentials than new samples in fresh solutions.

Data for Alloy 22 samples of various ages in both fresh and aged SAW solutions are shown in Table 3. Old samples and solutions were exposed in the Long-Term Corrosion Test Facility for 4 years. New samples and solutions were not exposed in the Long-Term Corrosion Test Facility prior to the test. Old Alloy 22 samples appear to have a higher corrosion potential than new samples. This may be due to either a transformation in the passive film or the deposition, on the

surface of the sample, of dissolved metals such as iron, which may have come from iron-containing samples other than Alloy 22 tested simultaneously in the Long-Term Corrosion Test Facility.

Table 3. Approximate Corrosion Potential of Alloy 22 Samples of Various Ages in Fresh and Aged Brine Solutions

Alloy 22 Sample	Solution	Temp. °C	E_{corr} mV vs. SCE
New	New SAW	90	–170
New	Old SAW	90	+40
Old	New SAW	90	+370
Old	Old SAW	90	+320

Data for Alloy 22 samples of various ages in aged solutions from the Long-Term Corrosion Test Facility are summarized in Table 4. The elevation of the open circuit corrosion potential measured in SAW is most likely due to the dissolution of metal ions from samples (and fixtures) in the Long-Term Corrosion Test Facility in this relatively acidic solution. For example, iron and nickel were detected at approximately 5 and 20 mg/L, respectively. In the case of these SAW measurements, it is important to note that the corrosion potential was independent of sample age. The sample exposed for four years in the Long-Term Corrosion Test Facility has the same corrosion potential as a new sample. Thus, no change attributable to the passive film was observed.

Table 4. Approximate Corrosion Potential of Alloy 22 for Various Sample Ages in Aerated Aged Solutions Taken from the Long Term Corrosion Test Facility

Solution	Conc.	Acidity	Temp.	E_{corr} at ~0 y	E_{corr} at ~1 y	E_{corr} at ~4 y
	× J-13	pH	°C	mV vs. SCE	mV vs. SCE	mV vs. SCE
SAW	1000	3	90	+330	+330	+305
SDW	10	10	90	–185	-85	+20
SCW	1000	11	90	–275	-185	–60
BSW	50,000	13	105	–710	+0	

NOTE: BSW = Basic Saturated Water

Lesser elevations in corrosion potential were observed in other solutions. However, in these cases, it is unclear whether the changes were due to the solution or the passive film. While the observed increases in corrosion potential may decrease the differential potential, thereby lowering the overall resistance to localized corrosion, a substantial differential still exists. Furthermore, the time dependence of the critical potential for localized attack has not been determined.

Corrosion Potential in SAW at 90°C (194°F)—Additional measurements of the corrosion potential of Alloy 22 in SAW at 90°C (194°F) have been made at Lawrence Livermore National

Laboratory. Open circuit corrosion potentials were measured under different aeration conditions. A standard Ag/AgCl reference electrode was used. After 24 hours, cyclic polarization measurements were made. Each experiment was replicated twice. In this case, the specimens were ¼-inch diameter rods with a length of 12 inches (30 cm). Approximately 1 in. (2.5 cm) of the sample was below the water line in the cell, corresponding to a wetted surface area of approximately 5.38 cm^2. Tests were conducted with variable amounts of dissolved oxygen. Tests conducted with electrolytes that were purged with air are referred to as aerated, whereas tests conducted with electrolytes that were purged (stripped) with nitrogen are referred to as deaerated. Tests conducted without air or nitrogen purging are referred to as undeaerated. Table 5 shows a summary of these recent results.

Table 5. Corrosion Potentials for Alloy 22 Rods in SAW at 90°C after 24 Hours

	1st E_{corr} mV Ag/AgCl	2nd E_{corr} mV Ag/AgCl	Avg. E_{corr} mV Ag/AgCl	Avg. i_{pass} at 500 mVA cm^{-2}	E_{crit} mV Ag/AgCl
Aerated	-30.2	-21.8	-26.0	3.885×10^{-6}	+672
De-aerated	-299.2	-303.4	-301.3	1.431×10^{-5}	+647
Undeaerated	-79.9	-115.8	-97.9	4.501×10^{-6}	+665

All potentials are given in mV versus a standard Ag/AgCl reference electrode. The potential E_{crit} is defined as the potential at which there is a permanent increase in current density above the threshold passive current density of 2×10^{-5} A cm^{-2}. Figure 5 shows the increase of the open circuit corrosion potential of Alloy 22 with time under different aeration conditions.

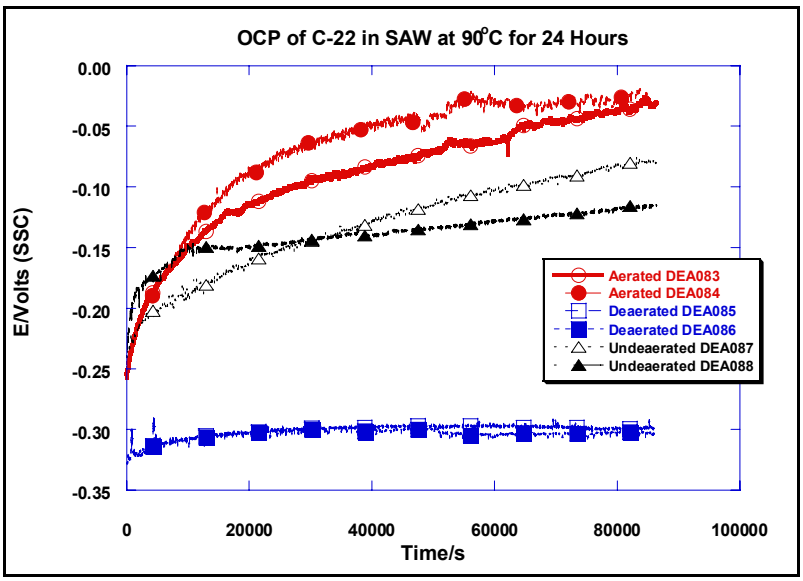

Figure 5. Open Circuit Corrosion Potential of Alloy 22 (C-22) in SAW at 90°C

Figure 6 shows the cyclic polarization curves of Alloy 22 in SAW at 90°C (194°F) under different aeration conditions. As can be seen from Table 5, the potential at which the permanent current rise from background occurs under all three conditions is similar. Transpassivation was

observed under the deaerated and undeaerated conditions. This conclusion was drawn because the electrolyte color changed from clear before the polarization scan started to yellowish green at the end. However, E_{crit} cannot be said to be the transpassivation potential with a high degree of confidence since the experiment did not distinguish between the transpassivation potential and the oxygen evolution potential. From the literature, at a pH~3, O_2 evolution is expected to start at between 1000 and 800 mV versus Ag/AgCl. Samples of the resultant solution have been saved for further analyses.

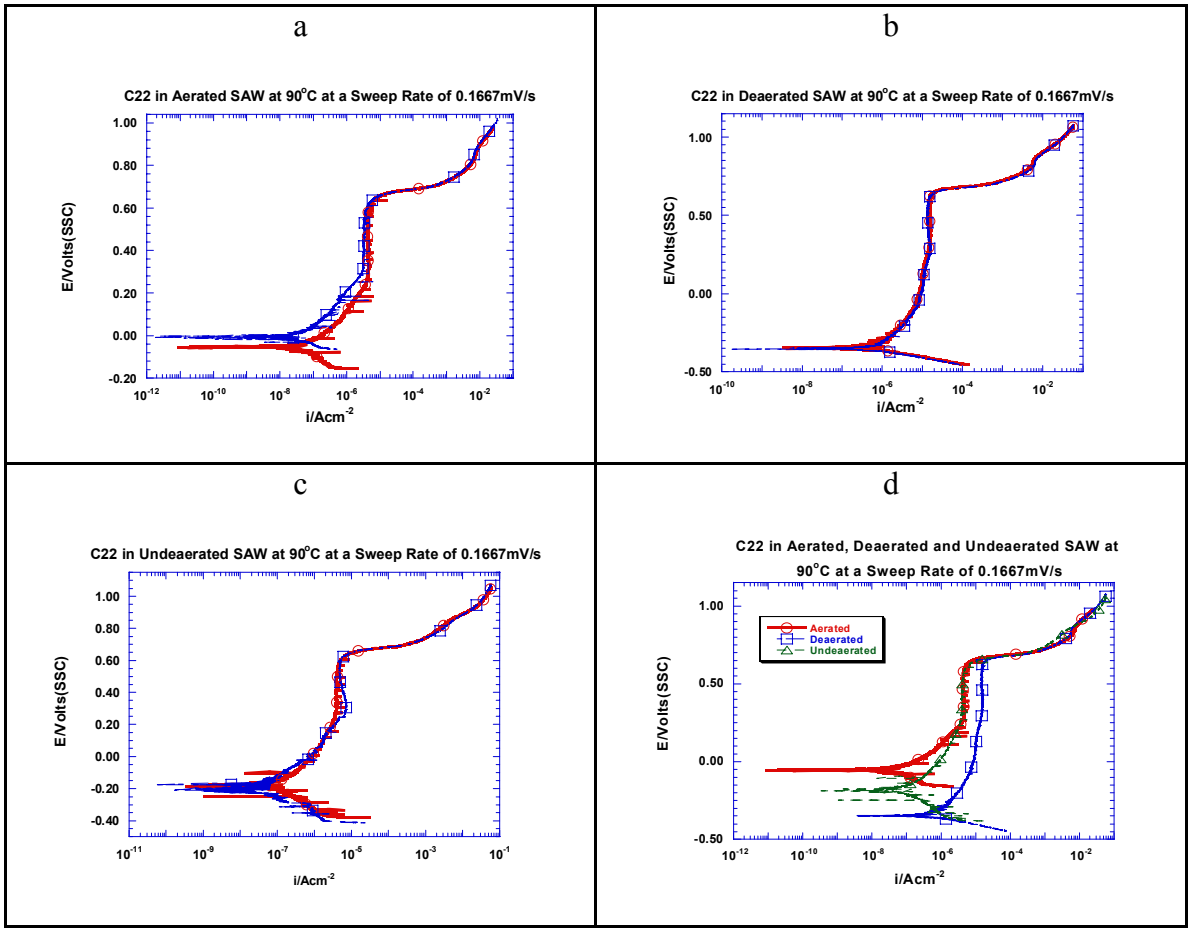

Figure 6. Polarization Curves of Alloy 22 (C-22) in (a) Aerated SAW, (b) De-Aerated SAW, and (c) Undeaerated SAW, all at 90ºC. A comparison of (a), (b) and (c) is shown in (d), the fourth frame

3.3.4 Structure of the Passive Film in Air and Brine

Oxide Films Formed in Air by Lawrence Livermore National Laboratory—Tunneling atomic force microscopy has been used to determine the steady-state thickness of the oxide film formed on Alloy 22 in air at 200°C (392°F). These measurements indicate that the thickness of this film is approximately 34 Å (3.4 nanometers). As can be seen from the subsequent discussion, the thickness of this film is similar to the passive film formed in brine solution.

Oxide Films Formed in Brine by GECRD—The passive films on both Alloy 22 and Titanium Grade 7 were about 50 Å (5 nanometers) thick after immersion in the GECRD test solution (Table 2) at 95°C (203°F) for two weeks (Kim et al. 2001). The relative abundances of alloying elements in the passive film were determined with X-ray photoelectron spectroscopy, as shown in Figure 7. As expected, oxygen had the greatest abundance, followed by silicon, nickel, chromium, molybdenum, and tungsten. The relatively high concentration of silicon is indicative of a silicate deposit (SiO_2). The abundance of nickel is probably associated with the presence of Ni_2O_3, $Ni(OH)_2$, and related species. The abundance of chromium is believed to be due to Cr_2O_3, or a mixed transition metal oxide containing large amounts of chromium. It must be noted that X-ray photoelectron spectroscopy can be used to determine elemental composition and oxidation states. However, the inference of a specific oxide structure based upon X-ray photoelectron spectroscopy is speculative at best. Other techniques, such as electron beam diffraction or low-angle X-ray diffraction should be employed for structural determinations.

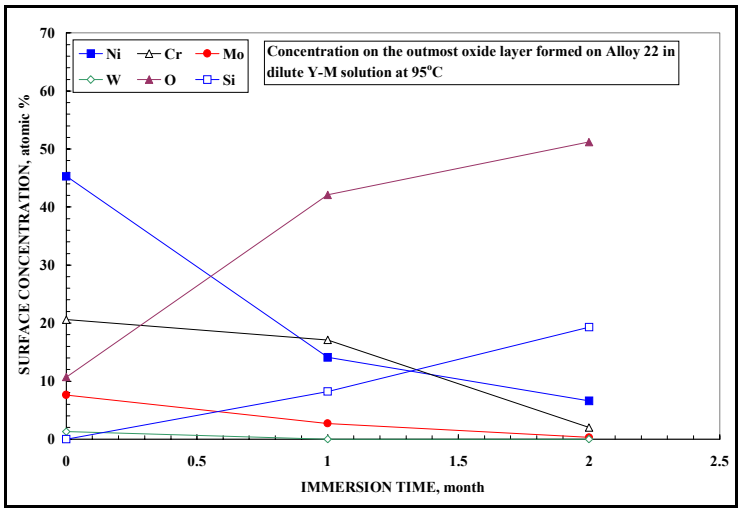

Figure 7. Steady State Passive Film Composition on Alloy 22 as a Function of Immersion Time Measurements made with X-Ray Photoelectron Spectroscopy

The presence of silicates on the surface is consistent with data published by Lawrence Livermore National Laboratory in *General Corrosion and Localized Corrosion of Waste Package Outer Barrier* (CRWMS M&O 2000c), and is therefore considered corroborative. Specifically, see Figures 28 and 29 of *General Corrosion and Localized Corrosion of Waste Package Outer Barrier* (CRWMS M&O 2000c), which show atomic force microscopy of silicate deposits, and an X-ray diffraction pattern of such a deposit. These data are the basis of the silicate deposit correction of corrosion rates.

Oxide Films Formed in Brine by Lloyd and Shoesmith—Lloyd and Shoesmith presented X-ray photoelectron spectroscopy data for passive films formed on Alloy 22 in 1M NaCl at pH~1 and 85°C (185°F) at Stainless Steel World 2001. These data indicate that the passive film is approximately 30 Å (3 nanometers) in this environment, which is roughly consistent with the data from GECRD for passive films in simulated 2,800× J-13 solutions at 95°C.

3.3.5 Oxide Films Formed during Dry Oxidation

Dry Oxidation of Alloy 22—A sample of Alloy 22 was oxidized at 550°C (1,022°F) for 10,000 hours. A cross section of the oxide film formed on this sample was then imaged with transmission electron microscopy and analyzed by energy dispersive spectroscopy of X-rays. Energy filtering was used to generate elemental maps like the one shown in Figure 8. From these data, it appears that a chromium-rich film forms directly on the surface of the Alloy 22 with a film rich in iron and nickel formed on the outermost surface. The entire surface layer is approximately 500 Å (50 nanometers) thick. The chromium-rich region is about 1/3 of the overall layer thickness. This structure is similar to that inferred from the X-ray photoelectron spectroscopy studies of passive films formed in brine by GECRD.

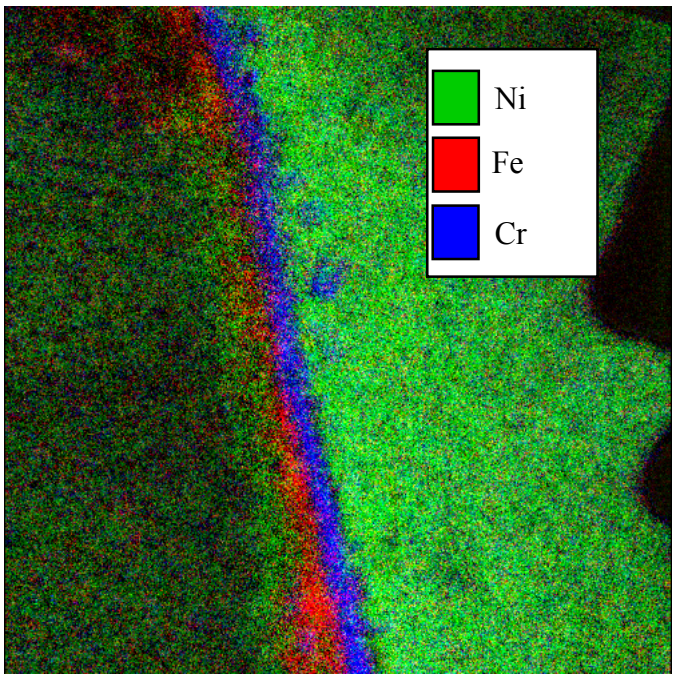

Note: Energy-filtered images for iron, nickel, and chromium. The epoxy mount is shown on the far left, with the oxide film being represented by the multi-colored bands in the center of the image, and the alloy shown as the bright green region to the far right.

Figure 8. Alloy 22 Oxidized at 550°C for 10,000 Hours

Conclusions—The relevance of this new work is best understood by reviewing it in the context of data previously published for dry oxidation in *General Corrosion and Localized Corrosion of Waste Package Outer Barrier* (CRWMS M&O 2000c, Section 6.1). An empirical model based upon data presented for dry oxidation of chromium-containing steels is given in this reference document. This model is based upon data published by Welsch et al. (1996, p. 169, Figure 25). This text suggests that Cr_2O_3 growth obeys the parabolic (Wagner) law at high temperature. An upper bound of the rate constant is represented in *General Corrosion and Localized Corrosion of Waste Package Outer Barrier* (CRWMS M&O 2000c, Equation 13). Applying this bounding rate constant to the oxidation of Alloy 22 at 550°C (1,020°F) for 10,000 hours, the thickness of the Cr_2O_3 layer should be less than 2,700 Å (270 nanometers). Since the observed thickness is less than 500 Å (50 nanometers), the data are considered corroborative. Based upon the same set

of data in Welsch et al. (1996, p. 158, Figure 18), the lower bound for the rate constant yields a film thickness of 270 Å (27 nanometers), which is also considered to be corroborative.

3.4 GENERAL AND LOCALIZED CORROSION

Corrosion is one of the most important degradation modes for the waste package and drip shield. Corrosion will only occur, however, when a conducting electrolyte (e.g., salt solution) is present. Under dry conditions, corrosion will not be a viable degradation mode for the waste package or drip shield. During the wet periods of emplacement, more than one type of corrosion may occur. Depending on the electrochemical potential that the package would achieve over time, corrosion modes could be broadly categorized into (1) general or passive corrosion and (2) localized corrosion. General or passive corrosion is the slow and relatively uniform thinning of materials. General corrosion will occur at electrochemical potentials that are low enough for the alloys to maintain their passivity. Localized corrosion is the uneven dissolution of the alloy. That is, during localized corrosion certain areas of the metal may corrode while other areas remain passive or unattacked. Localized corrosion occurs at an electrochemical potential that is higher than a critical potential for the breakdown of passivity. Because no additional data have been obtained for titanium, only data related to corrosion of Alloy 22 will be discussed in this section.

3.4.1 General or Passive Corrosion

Alloy 22 relies on the formation of a thin, relatively impervious oxide film on its surface for protection against wet corrosion. Previous short-term laboratory testing showed that under environmental conditions that would be typical of a repository at Yucca Mountain, Alloy 22 would remain passive and therefore have an insignificant thinning rate. Figure 9 shows the current density measured on Alloy 22 when a constant potential of E_{corr} + 100 mV was applied to specimens immersed in SCW at 90°C (194°F) and in 0.028 M NaCl at 95°C (203°F). For both environments, the passive current density decreased as the time increased [Scientific Notebook #LLNL-SCI-452-VII]. Figure 9 also shows the fitting of the experimental data by a power law. The decrease in current density seems faster in the sodium chloride solution than in the simulated water solution. The experimental results in Figure 9 are single tests. However, this preliminary data show that after 1 week of testing, the measured electrochemical current predicted a maximum corrosion rate of 0.3 μm/year in the NaCl solution and a maximum corrosion rate 1.6 μm/year in the SCW solution. This is described as a maximum corrosion rate since part of the current density represented in Figure 9 could be a consequence of confounding redox reactions on the surface of the sample. Data in Figure 9 show that, under small anodic activations, Alloy 22 maintains its passivity and that it is likely that the current density will decrease as the exposure time increases. Similar behavior was found by Lloyd (2001), who studied the effect of applied potential on the current density of Alloy 22 exposed to 0.1 M NaCl + 0.1 M H_2SO_4. She reported that, when an anodic potential was applied to Alloy 22 in this acidic solution, the current density decreased continuously as the time increased.

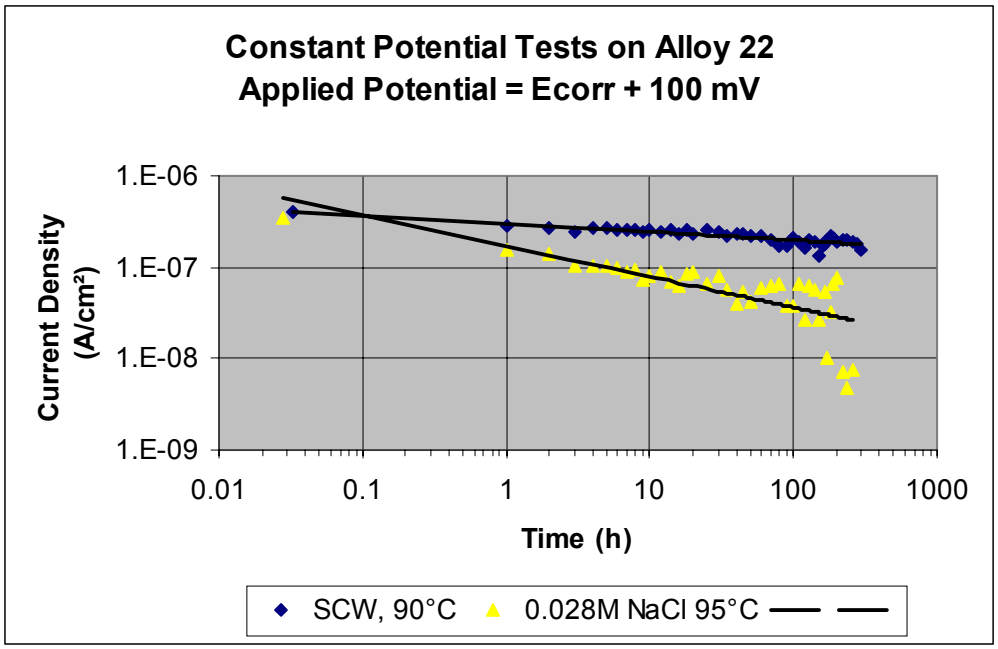

Figure 9. Constant Potential Tests of Alloy 22

3.4.2 Localized Corrosion

Alloys that rely on a passive film for protection against corrosion may be susceptible to localized corrosion under severe environmental conditions. Alloy 22 is one of the most resistant alloys to localized corrosion in the Ni-Cr-Mo family of alloys. Localized corrosion includes pitting corrosion and crevice corrosion. Pitting corrosion is the formation of corroded cavities on the freely exposed surface of a passive metal. Crevice corrosion is the preferential dissolution of a metal that is exposed to an occluded environment, for example, under a gasket or inert deposits. The main environmental variables that control the occurrence of localized corrosion are electrochemical potential, chloride concentration and temperature. The higher these variables are, the higher the aggressiveness of the environment towards localized corrosion. It is accepted that Alloy 22 is extremely resistant to pitting corrosion, even in the harshest of environments. However, there is experimental laboratory evidence that this alloy may be susceptible to crevice corrosion under highly aggressive conditions. For example, Alloy 22 would suffer crevice corrosion under tight crevices formed with the aid of polytetrafluoroethylene (PTFE) in pure saturated chloride near the boiling point and at electrochemical potentials in the range of oxygen evolution (electrochemical instability of water). It can be inferred that if the corrosion potential of Alloy 22 were maintained below the electrochemical potential for oxygen evolution, localized corrosion would not occur.

Figure 10 shows the potentiodynamic polarization of four Alloy 22 U-bend specimens in SAW at 90°C (194°F) (Scientific Notebook #LLNL-SCI-452-VII). Each U-bend specimen contained two PTFE-formed crevices. Although the corrosion potential for the samples tested for 4 years in the Long-Term Corrosion Test Facility were higher than unexposed samples, the passive current density is approximately 2 orders of magnitude lower. Also, in Figure 10, even though the corrosion potentials of the specimens were different, all of them had a similar potential for

the breakdown of the passive region. Although the four specimens were exposed to electrochemical potentials near 1 V SSC (silver-silver chloride) and to current densities on the order of 10 mA/cm², none of them suffered crevice corrosion in the tested solution. The corrosion potentials of the specimens in Figure 10 were different from each other because the surface condition of the specimens and the composition of the electrolyte solution were different.

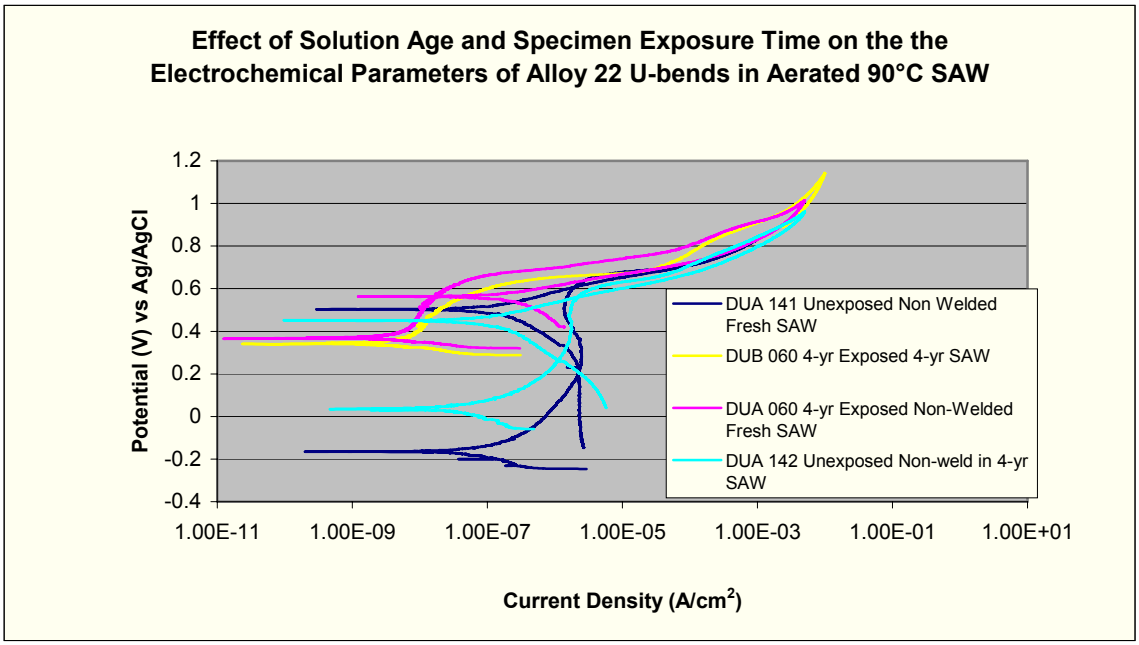

Figure 10. Potentiodynamic Polarization of Alloy 22 U-Bend Specimens in SAW at 90°C

Table 6 shows a series of experiments in which the corrosion potential of metallic electrodes is being monitored as a function of time (Scientific Notebook #LLNL-SCI-460-VI). These electrodes include Alloy 22 U-bend specimens, both fresh (as-received or untested) and those that were removed from the Long-Term Corrosion Test Facility, and platinum electrodes. These specimens are being exposed to electrolyte solutions that were removed from the Long-Term Corrosion Test Facility, that is, solutions that may contain dissolved corrosion products from metallic specimens that were immersed in them for as long as 4 years.

Table 6. Monitoring of the Corrosion Potential of U-bend Alloy 22 Specimens and Platinum Rods in Electrolyte Solutions Removed from the Long-Term Corrosion Test Facility

Specimen ID	Environment	Weeks Pre-exposed in LTCTF	Weeks of Monitoring Corrosion Potential (Top Bench)	Corrosion Potential at Week of Exposure in the Previous Column in mV, SSC
DUB 028	SAW, 60°C	218	25	339
DUB 157	SAW, 60°C	0	25	340
Pt Rod	SAW, 60°C	0	25	348
DUB052	SAW, 90°C	216	25	275
DUB159	SAW, 90°C	0	25	322

Table 6. Monitoring of the Corrosion Potential of U-bend Alloy 22 Specimens and Platinum Rods in Electrolyte Solutions Removed from the Long-Term Corrosion Test Facility (Continued)

Specimen ID	Environment	Weeks Pre-exposed in LTCTF	Weeks of Monitoring Corrosion Potential (Top Bench)	Corrosion Potential at Week of Exposure in the Previous Column in mV, SSC
Pt Rod	SAW. 90°C	0	25	333
DUB088	SCW, 60°C	214	25	17
DUB156	SCW, 60°C	0	25	-53
Pt Rod	SCW, 60°C	0	25	35
DUB112	SCW, 90°C	209	25	-52
DUB161	SCW, 90°C	0	25	-120
Pt Rod	SCW, 90°C	0	25	-70
DUB128	SDW, 60°C	209	25	-11
DUB160	SDW, 60°C	0	25	-147
Pt Rod	SDW, 60°C	0	25	194
DUB132	SDW, 90°C	208	25	16
DUB162	SDW, 90°C	0	25	-29
Pt Rod	SDW, 90°C	0	25	16
ARC22U-20	BSW, 105°C	58	23	29
DUB 163	BSW, 105°C	0	23	-56
Pt Rod	BSW, 105°C	0	23	91

NOTE: LTCTF = Long-Term Corrosion Test Facility.

Some observations from the results in Table 6 are as follows:

1. The corrosion potential of specimens in SAW (acidic) are in general 200 to 300 mV higher than the corrosion potential of specimens exposed to the other solutions (alkaline). As discussed in Section 3.3, it can be inferred that this SAW solution contains chemical species with a more anodic redox potential.

2. In general, the corrosion potential of the fresh Alloy 22 U-bend specimen is slightly lower than the corrosion potential of the old specimen. This may suggest that the old specimen was ennobled by the formation of a corrosion protective passive film on the surface.

3. In general, the platinum specimen tends to behave like the old Alloy 22 specimen.

4. In general, as expected, the corrosion potentials are lower at 90°C (194°F) than at 60°C (140°F) although the difference is small.

5. Table 6 shows that the corrosion potential of the Alloy 22 creviced specimens in SAW solutions are approximately 300 mV below the onset of passivity breakdown and those in SCW and BSW solutions are approximately 400 mV below the potential at which either transpassivity and/or oxygen evolution occurs.

In short, the experimental data show that it is unlikely that Alloy 22 may reach a critical potential and therefore fail by localized corrosion in environments relevant to a repository at Yucca Mountain.

3.5 STRESS CORROSION CRACKING

3.5.1 Stress Corrosion Crack Initiation Tests

Slow Strain Rate Tests—A variety of test methods have been employed including slow strain rate tests to establish a defensible threshold stress for SCC initiation. These slow strain rate tests involve the very slow straining of a tensile specimen exposed to the desired environment until the specimen ruptures. From comparison of fracture stress and strain values and fracture morphology to those of control specimens strained under the same conditions in an inert environment, it is possible to assess if SCC has initiated and the relative SCC resistance of the material under a range of environments, metallurgical conditions and applied potentials. By running a series of tests at increasing applied potentials it may be possible to establish a threshold potential (analogous to the crevice corrosion repassivation potential) below which SCC will not initiate or if initiated, will not propagate. In Table 7.3.3-3 in Volume 1 of the *FY01 Supplemental Science and Performance Analyses* (BSC 2001a), a number of slow strain rate test results were reported for Alloy 22 tested at a strain rate of 1.66×10^{-6} s^{-1} under a range of environments (4M NaCl, BSW [with and without nitrate and sulfate ions added], SCW and SAW [with and without lead ions added] over a range of applied electrochemical potentials. Both creviced and uncreviced specimens were tested. SCC initiation was reported in only one case, 98°C (194°F), 4M NaCl at a high applied potential of 400 mV versus Ag/AgCl.

Recent additional slow strain rate test runs are summarized in Table 7 along with selected tests run previously for comparison. As can be seen, Alloy 22 is extremely resistant to SCC initiation at the corrosion potential, E_{corr}, in the range of additional slow strain rate test environments evaluated which include saturated calcium chloride tested at 120°C (248°F), SAW with and without lead additions and BSW. In the case of 95°C (203°F) SCW at a potential of +400 mV (SSC), there are shallow appearing surface fissures on the specimen gage section that may be incipient stress corrosion cracks. Note, however, that the ductility and failure time of this sample (reduction in area at fracture) are comparable to those of the sample tested in air. It is possible that these features are not cracks but sites of preferential etching such as might occur at dislocations.

Table 7. Alloy 22 Slow Strain Rate Test Results (Strain Rate: ~$1.66 \times 10^{-6}\ s^{-1}$)

Sample	Environment	Temp. (°C)	E_{corr} (SSC)	$E_{applied}$ (SSC)	Time to Failure (h)	UTS (ksi)	RA (%)	Observations – Stereomicroscope X 40
012	Air	20	N/A	N/A	124	114	74	
004 HC	Sat. $CaCl_2$, pH ~ 6	120	-140 to -180	E_{corr}	~~127~~	109	71	No SCC.
015HC	SAW, pH~3	63	-7 to +360	E_{corr}	118	110	79	No SCC
003 HC	SAW + . 005% $Pb(NO_3)_2$, pH ~ 3	95	-90 to +400	E_{corr}	118	109	85	No SCC.
127HC	BSW, pH~13	98	-240	E_{corr}	123	108	72	No SCC
020 HC	SCW, pH ~ 9	95	-109	+400	116	116	85	Possible incipient SCC. SEM underway

NOTES: Strikethrough times correspond to straining times. E_{corr} = corrosion potential. UTS = ultimate tensile stress. RA = reduction in area at time of rupture. SSC = silver-silver chloride. HC = Halar coating-crevice. BSW = basic saturated water. SAW = simulated acidified water. SCW = simulated concentrated water. Halar is a polymeric coating material used to create specimen crevices.

Single U-Bend and Double U-Bend Test—U-bend specimens are formed by bending rectangular strips 180 degrees over a rounded mandrel and then restraining the straight legs using insulated bolts. The bending process results in ~12 percent plastic strain (cold work) at the apex and applied stresses greater than the initial yield strength of the material. For the double U-bends, two strips are bent over the mandrel simultaneously forming a very tight crevice between them with ~5-7 percent plastic strain at the apex. The single U-bends were formed from annealed Alloy 22 and Titanium Grade 16 sheet materials and included both annealed base metal and welded samples with the weld located at the apex of the U-bends. The single U-bends were exposed for times up to one year in the Long-Term Corrosion Test Facility at 60° and 90°C (140° and 194°F) in SAW, SCW and SDW environments. Postexposure, stereomicroscopic examinations were performed on a number of Alloy 22 specimens with no evidence of stress corrosion cracking. Selected Alloy 22 U-bend specimens exposed to the aqueous phase and removed from the 90°C (194°F) SAW tank environment after four years exposure were also examined stereomicroscopically with no evidence of SCC. Also, two Alloy 22 and two Titanium Grade 7 creviced double U-bend specimens were disassembled to reveal the stressed creviced areas and were examined stereomicroscopically exposure to 105°C (221°F) BSW with no evidence of SCC after 17 and 18 months, respectively. The absence of crack initiation, in these relatively long-term, above-yield stress tests, supports the use of an initiation stress threshold value considerably above the currently used value.

Constant Load Tests—The constant load test is the most direct technique for establishing the dependence of crack initiation time on applied stress. This stress dependency can then be used to estimate the threshold initiation stress below which SCC is not expected to occur. For this test

series, uniaxially loaded specimens of Alloy 22 and Titanium Grade 7 were exposed at 105°C (221°F) to a concentrated (~7500-fold concentration), aerated J-13 environment, pH = 12.4 for >4000 hours along with comparison alloys (Types 304 and 316 nuclear grade stainless steels). Alloy 22 was tested in several conditions: as-received, aged to produce tetrahedrally close-packed phases (175 hours at 700 C [1,300 F]), aged to produce long-range ordering (1,000 hours at 520 C [970 F]), cold worked 20 percent, cold worked 20 percent plus aged to produce long-range ordering, creviced, aged to produce tetrahedrally close-packed phases and creviced, and welded. Titanium Grade 7 was tested in the as-received and creviced conditions. Alloy 22 was loaded at 586 and 641 MPa and Titanium Grade 7 was tested at 276 and 310 MPa. No SCC occurred during the >4000 hour exposure period for any of the range of metallurgical conditions tested. Selected specimens of the annealed Alloy 22 material were stressed to over twice the yield strength level and in fact to as high as 690 MPa versus an ultimate tensile strength of 718 MPa and yield strength of 324 MPa with no evidence of SCC. This is consistent with an extremely high resistance to crack initiation. As-welded Alloy 22 specimens were stressed to as high as 641 MPa with no SCC. In contrast to Alloy 22, Titanium Grade 7 did fail in times as short as ~350 hours by apparent stress corrosion at applied stresses as low as 276 MPa compared to a yield strength of 248 MPa and an ultimate tensile strength of 365 MPa.

3.5.2 Stress Corrosion Crack Propagation Tests

Fatigue precracked (to form a sharp crack tip at the notch) compact tension fracture mechanics type specimens were employed to evaluate Alloy 22 and Titanium Grade 7 crack growth rates versus applied stress intensity factor, K_I, and to estimate the threshold stress intensity, K_{ISCC}. Both annealed and 20 percent cold-worked specimens of each material were evaluated in 110°C (230°F) BSW: Titanium Grade 7 at a stress intensity of 30 MPa $m^{1/2}$ and Alloy 22 at stress intensities of 30 MPa $m^{1/2}$ and 45 MPa $m^{1/2}$. In addition, annealed Alloy 22 was evaluated in 95°C (203°F) SAW and SCW at a stress intensity of 45 MPa $m^{1/2}$. To accelerate SCC initiation at the fatigue crack tip, during the initial portion of each individual test, the applied load and resulting stress intensity were cycled with a trapezoidal wave form with an initial cyclic frequency of either 0.01 or 0.001 Hz, a slow ramp up to the maximum load, and a ramp down to generally 70 percent of maximum load. The hold time at maximum load was gradually increased in steps during the test and, assuming the crack continued to grow with each longer-hold time step, the load was then held constant for a sustained period to obtain the SCC "constant-load" growth rate for a given K_I value. With Alloy 22, sustained crack growth has not yet been obtained for annealed material in the BSW environment at K_I values as high as 45 MPa $m^{1/2}$. However, sustained growth was obtained for 20 percent cold-worked Alloy 22 material loaded to 30 MPa $m^{1/2}$ with an extremely low measured crack growth rate of 2×10^{-10} mm/s. In contrast, in BSW, annealed Titanium Grade 7 exhibited sustained crack growth at 30 MPa $m^{1/2}$ with a significantly higher, but still very low, crack growth rate of 1×10^{-8} mm/s. In SCW and SAW, annealed Alloy 22 did sustain constant-K_I crack growth at 45 MPa $m^{1/2}$ with average growth rates of 2×10^{-10} mm/s and 5×10^{-10} mm/s, respectively. These constant-load growth rates are indicated for all three environments on a plot of crack growth rate versus stress intensity in Figure 11. Also shown on this plot are calculated constant repassivation parameter, n, curves for a range of n values between 0.8 and 1.4. As can be seen, for Titanium Grade 7 in the BSW environment, an n value of 0.8 appears conservative. For Alloy 22, n values between slightly less than 1.2 and 1.4 appear to bracket the values obtained in the range of environments

evaluated. These results provide a basis for raising the uniform distribution range of the Alloy 22 *n* value used in the TSPA-SR model (between 0.75 and 0.84) and in the supplemental TSPA model (0.843 to 0.920) to still higher values which will significantly extend the through-wall cracking time once SCC initiates.

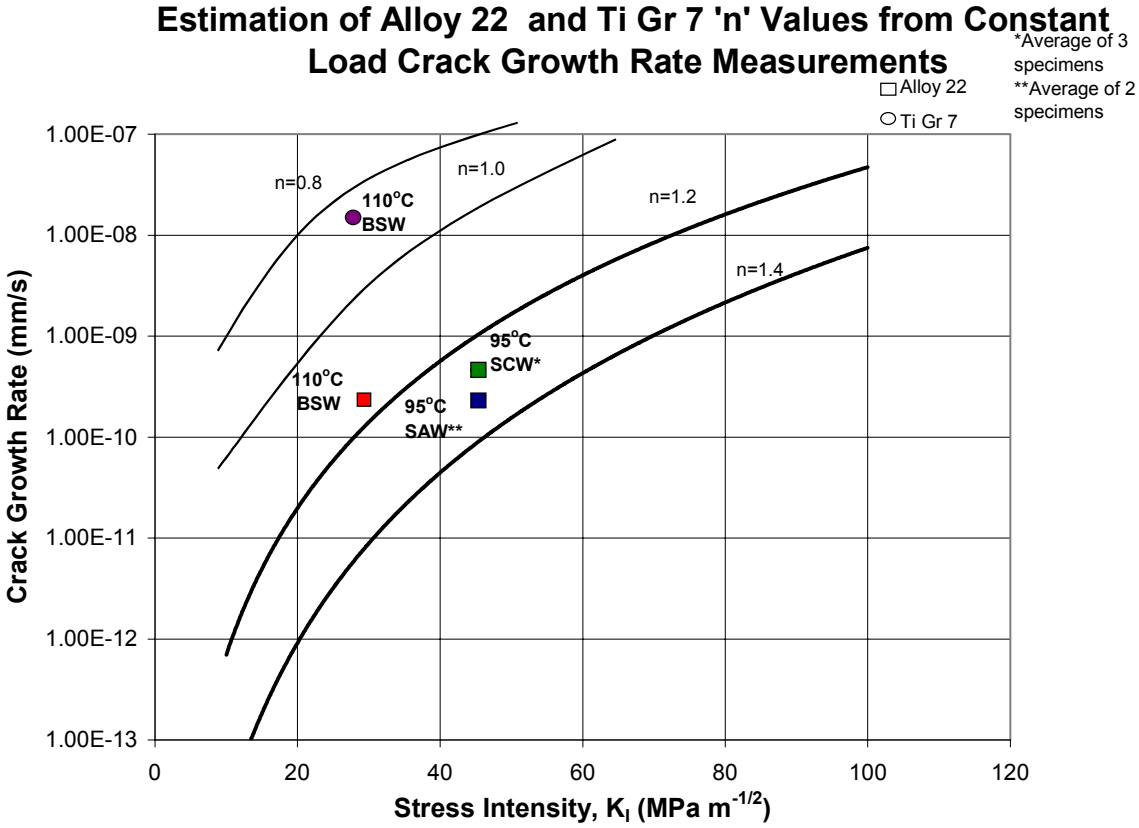

Figure 11. Estimation of Exponent '*n*' from Crack Growth Rate Measurements in a Range of Relevant Environments

With respect to estimation of the critical stress intensity factor, K_{ISCC}, the available results allow setting an upper bound value of 30 MPa $m^{1/2}$ in BSW at temperatures up to at least 110°C (230°F) and an upper bound value of 45 MPa $m^{1/2}$ in SAW and SCW at temperatures up to at least 95°C (203°F). However, it may prove very difficult to establish actual threshold values since at lower K_I levels, the test times become extremely long to obtain measurable crack growth.

3.6 STRESS MITIGATION AND WELD STRESS MEASUREMENT

As discussed in Section 3.5, SCC is a potential degradation mode that can result in penetration of the waste package outer barrier (Alloy 22). SCC of materials may occur when an appropriate combination of material susceptibility, tensile stress, and environment is present. The current design specifies that all stresses including weld residual stresses from the fabrication of the waste package outer barrier (except the waste package closure welds) and the Titanium Grade 7 drip

shield be fully relieved by solution annealing. Therefore, it is assumed that those components are not subject to SCC (CRWMS M&O 2000e, Section 5). To mitigate the potential for early failure by SCC, the closure of the waste package outer barrier is designed to include two lids with two separate post-weld stress mitigation processes: local induction annealing of the outer-lid closure weld and laser peening of the inner-lid closure weld. These postweld processes are designed to mitigate tensile residual stresses and generate compressive stresses at the surface down to a significant depth. The stress mitigation treatments are limited to the closure weld area. In particular, the induction annealing is performed in such a way to minimize heating of other areas to undesirable temperatures. This section summarizes the testing and analysis results of the stress mitigation processes including recent residual stress measurements.

Local Induction Annealing—Induction annealing causes local heating that allows for the relief of the residual stresses caused by welding. Quenching, which cools the surface faster than the inner material, results in compressive residual stresses on the surface. More details of the local induction annealing operations are discussed in *Stress Corrosion Cracking of the Drip Shield, the Waste Package Outer Barrier, and the Stainless Steel Structural Material* (CRWMS M&O 2000e, Section 6.2.2.4). Several induction-annealing tests were conducted at the facility of subcontractor Ajax Magnethermic Corporation since May 2001. The tests were designed to evaluate and optimize the process parameters and to demonstrate the feasibility of induction annealing for stress mitigation of the waste package closure welds.

Two planar mockups were induction annealed and quenched using water or forced air. Temperature measurements were made at key locations to determine time-temperature history. In addition, the resulting residual stresses were measured using the ring-core method by subcontractor Lambda Research Incorporated. The entire heating and quenching cycle was performed in approximately 16 minutes. At the hottest thermocouple location, heating to 1,120°C (2,048°F), the target temperature, was achieved in approximately 7 minutes, and quenching to 500°C (932°F) in approximately 2 to 3 minutes. The total time, during which the temperature at any location was above 500°C (932°F), was approximately 9 to 10 minutes (the target time was less than 10 minutes). No appreciable difference in the time-temperature history was observed between the forced air-cooled sample and water-cooled sample. The residual stress was measured at the weld to a depth of 5-mm and found to be compressive to at least this depth.

Laser Peening—As discussed above, laser peening has been proposed to mitigate stresses and generate compressive stresses at the surface and down to a significant depth in the closure weld region of the inner lid of the Alloy 22 waste package outer barrier. Several thick plate Alloy 22 weldments have been fabricated for laser peening process development at Lawrence Livermore National Laboratory. The efforts are currently geared toward optimizing the process parameters to maximize the depth of compressive stresses.

The laser peening technique has been used in a variety of industrial applications to mitigate SCC of materials. Recently Toshiba Corporation has developed a fiber optic delivery system (approximately 40-m [131-ft] run) for the in situ laser peening of BWR core shroud welds in order to prevent SCC (Sano et al. 2000; Sano et al. 2001). The feedback-controlled beam tracking system ensures beam placement within ±0.1 mm at the end of the 40-m (131-ft) run.

The Toshiba system has been in production since 1999 and has successfully peened welds at two nuclear power stations in Japan.

3.7 WASTE PACKAGE MATERIALS PERFORMANCE PEER REVIEW

During the second half of fiscal year 2001, in response to DOE direction, Bechtel SAIC Company initiated a consensus peer review of the waste package materials performance. The objectives of this peer review are to:

- Review the current bases for predicting long-term corrosion performance of Alloy 22 waste package and Titanium Grade 7 drip shield materials and the ongoing and planned experimental and modeling program to increase confidence in the long-term performance projections;

- Recommend any augmentations of existing and planned tasks or additional tasks to significantly strengthen the program; and

- Prepare an interim and a final report of the Panel's assessment of the adequacy of the current and planned program and assist DOE in prioritizing future work plans.

To conduct this peer review, an independent panel of seven experts in the materials science and engineering disciplines was selected. One of the seven was to serve as the Chairman of the Panel. The seven Panel members are also assisted by an international group of 15 subject matter experts in various areas.

A kickoff meeting was held on May 23 to launch the peer review with the Project staff making presentations to the Panel on technical areas of concern. The presentations included data and models that form the technical basis for waste package performance predictions. Subsequent to the kickoff meeting, the Panel also had a number of meetings with the Project staff on different subjects including localized corrosion, fabrication issues, stress corrosion cracking, and environment on the waste package and drip shield. The Panel also had an open meeting with presentations from the representatives from the State of Nevada and the U.S. Nuclear Regulatory Commission. Based on the information gathered from these meetings and detailed review of the Project documents—the *Waste Package Degradation Process Model Report* (CRWMS M&O 2000a) and the supporting AMRs—the Panel produced an interim report of their findings (Beavers et al. 2001). These findings were formally presented to the Project in a public meeting on September 25, 2001.

Preliminary Findings from Peer Review—Overall, the Panel has not found any technical basis for concluding that the waste package materials would be unsuitable for long-term containment. While significant technical issues remain to be settled, likelihood is great that the uncertainty about long-term performance can be substantially reduced through further experiments and analysis. The Panel also found that the Project has a sound approach for corrosion control.

The Panel concluded that corrosion is the most significant potential degradation mode and three important environmental conditions that affect the corrosion behavior processes are moist dust on the metal surface, scale and deposits on the metal surface and metal-to-metal contact areas.

The Panel recommended that the Project adopt a comprehensive experimental and analytical modeling program for all three environmental conditions.

The Panel members have reviewed the available data on the passive corrosion rates of Alloy 22 and Titanium Grade 7 and found that, in principle, the rates could remain low enough for waste packages to survive for thousands of years. However, whether or not this happens depends on what changes take place in the protective passive films. The Panel believes that any changes in the passive film could be due to changes in the intrinsic nature of the film, changes in the environment or changes in the alloy itself (e.g., phase transformations). The Panel recognizes that some aspects of these areas are being studied by the Project while many of the others have not yet begun. The Panel will continue to review the planned work to assess the adequacy. The Panel also recommends that a back-up alloy and a comparison alloy be included in the experiments and analysis.

In the area of localized corrosion, the Panel considers that the approach taken by the Project in the evaluation of resistance to localized corrosion is appropriate. However, the Panel recommends that the Project conduct testing in aggressive environments that cause localized corrosion in order to examine the margins of corrosion resistance.

In the area of stress corrosion cracking, the Panel believes that the threshold stress criterion used in the model is not conservative. It is recommended that the stress threshold be replaced with a stress intensity factor threshold. In addition the panel recommends that the Project consider alternative models for stress corrosion cracking.

4. IMPLICATIONS OF RECENT TEST RESULTS AND OTHER ADDITIONAL INFORMATION

4.1 ENVIRONMENT ON THE DRIP SHIELD AND WASTE PACKAGE OUTER BARRIER

For the environment on the waste package and drip shield, the additional data, obtained through a literature search, suggest that a lower deliquescence point is needed to account for the possibility of mixed salts being present. Electrochemical corrosion processes can then be initiated by somewhat lower relative humidities. Initiation of general corrosion at lower relative humidities is not expected to significantly change the waste package lifetime. Susceptibility to localized corrosion may not occur at the deliquescence point of the mixed salts, but may occur, at least for sodium base salts, at substantially higher relative humidities, where the ratio of aggressive to inhibitor anions in the aqueous solutions is greater than a critical value. Sodium is expected to be the dominant cationic species in soluble salt deposits. Based on a literature review of trace element geochemistry, these elements are not expected to have a significant effect on corrosion either because of limited solubility (Pb and Hg) or because the enhancement of the corrosion process is not significant (As). Arsenic enhances hydrogen embrittlement but only when the material is already susceptible to hydrogen embrittlement under the conditions where As is present.

4.2 AGING AND PHASE STABILITY OF THE WASTE PACKAGE OUTER BARRIER

In the *Aging and Phase Stability of the Waste Package Outer Barrier* (CRWMS M&O 2001), only very qualitative data were available for assessing the stability of Alloy 22 at repository temperatures. Because these data were rather subjective, they had a large degree of uncertainty associated with them. The data, however, did not indicate that phase instabilities would occur under expected repository conditions. To account for the large uncertainty, a bounding argument was made, and it is for this bounding structure that the corrosion rate enhancement factor was applied. The data in Section 3.2 are quantitative, and the uncertainties that appear in Figure 2 are likely to be much smaller than those used in *Aging and Phase Stability of the Waste Package Outer Barrier* (CRWMS M&O 2001). The above data show that grain boundary precipitation will not occur at temperatures below 300°C (570°F). In addition, this approach is conservative because isothermal conditions are assumed even though temperatures in the potential repository are expected to peak at a temperature that will be determined by the thermal operating mode chosen for the potential repository (DOE 2001a, Sections 2.1.3 through 2.1.5), below 300°C (570°F) and perhaps as low as 85°C (185°F), within a few hundred years and decrease to very low values after that. The additional data suggest that the corrosion rate enhancement factor is not necessary for annealed Alloy 22 base metal.

4.3 PASSIVE FILM STABILITY

Additional data in the area of passive film characterization corroborate the present model and give no indication that long-term extrapolation of low passive corrosion rates is inappropriate.

4.4 GENERAL AND LOCALIZED CORROSION

Additional data in the area of general and localized corrosion indicate that no changes to the model are necessary.

4.5 STRESS CORROSION CRACKING

The full suite of recent test results reviewed above tends to support the currently used SCC process modeling approach. The recent experimentally obtained Alloy 22 and Titanium Grade 7 specific *n* values for the film rupture/repassivation model are more directly relevant than the previous values derived from stainless steel. These recent results indicate that the currently used *n* values are realistic for Titanium Grade 7 and are conservative for Alloy 22 leading to higher calculated crack growth rates than are actually expected. Further, the threshold SCC initiation stress range of 20 to 30 percent of yield strength appears to be conservative at least when no sharp cracks are present. This is true over the entire range of relevant environments evaluated including environments containing lead additions as well as saturated calcium chloride solutions at temperatures up to 120°C (394°F). Thus, the additional data indicate that the threshold stress for SCC initiation on smooth Alloy 22 samples could be higher than that used in the TSPA-SR model. The repassivation parameter, *n*, for crack growth by the slip dissolution model for SCC crack growth in Alloy 22 should be increased. Also, given the difficulty in sustaining crack growth in Alloy 22, the model should be modified to account for the arrest of crack growth once cracks are initiated.

There are no implications yet from the K_{ISCC} data.

4.6 STRESS MITIGATION AND WELD STRESS MANAGEMENT

The local induction annealing tests to date have demonstrated that the stress mitigation process is feasible and can induce compressive stresses from the surface to a significant depth in the closure-lid welds of the waste package outer barrier. The additional data do not have implications for the current model.

The laser peening technologies that are currently available for a variety of industrial applications, such as that developed by Toshiba (Sano et al. 2000; Sano et al. 2001), can be easily applied to the relief of the residual stresses at the surface of the waste package closure welds. These studies confirm our assertion that laser peening has been demonstrated as an effective stress mitigation process. There are no implications to the current model.

4.7 WASTE PACKAGE MATERIALS PERFORMANCE PEER REVIEW

The preliminary findings of the Peer Review Panel essentially confirm the Project's understanding of the data needs to strengthen the technical bases for the prediction of long-term corrosion performance of the waste package materials. Nevertheless, the impact of the Panel's recommendations on the TSPA-SR models is largely negligible because the current models include conservative and bounding approaches to account for the uncertainties and limitations in available data. The K_{ISCC} model for SCC initiation recommended by the panel has been carried as an alternate model to the stress threshold approach. This model can be adopted for situations when sharp cracks are present.

5. REFERENCES

AP-2.14Q, REV 2, ICN 0. *Review of Technical Products and Data.* Washington, D.C.: U.S. Department of Energy, Office of Civilian Radioactive Waste Management. ACC: MOL.20010801.0316.

AP-SIII.1Q, Rev. 0, ICN 1. *Scientific Notebooks.* Washington, D.C.: U.S. Department of Energy, Office of Civilian Radioactive Waste Management. ACC: MOL.20000516.0002.

Anderson, M.A.; Ferguson, J.F.; and Gavis, J. 1976. "Arsenate Adsorption on Amorphous Aluminum Hydroxide." *Journal of Colloid and Interface Science*, *54*, 391-399. New York, New York: Academic Press.

Anderson, L.C.D. and Bruland, K.W. 1991. "Biogeochemistry of Arsenic in Natural Waters: The Importance of Methylated Species." *Environmental Science and Technology, 25*, 420-427. Washington, D.C.: American Chemical Society.

Asphahani, A.I. 1980. "Localized Corrosion of High-Performance Alloys." *Materials Performance, 19*, (8), 555-559. Houston, Texas: National Association of Corrosion Engineers.

Barrow, N.J. and Cox, V.C. 1992. "The Effects of pH And Chloride Concentration on Mercury Sorption. I. By Goethite." *Journal of Soil Science, 43*, 295-304.

Beavers, J.A.; Devine, T.M., Jr.; Frankel, G.S.; Jones, R.H.; Kelly R.G.; Latanision, R.M.; and Payer, J.H. 2001. *Interim Report, Waste Package Materials Performance Peer Review Panel, September 4, 2001*. Las Vegas, Nevada: Waste Package Materials Performance Peer Review Panel. ACC: MOL.20011003.0369.

BSC (Bechtel SAIC Company) 2001a. *FY01 Supplemental Science and Performance Analyses, Volume 1: Scientific Bases and Analyses.* TDR-MGR-MD-000007 REV 00 ICN 01. Las Vegas, Nevada: Bechtel SAIC Company. ACC: MOL.20010801.0404; MOL.20010712.0062; MOL.20010815.0001.

BSC 2001b. *Environment on the Surfaces of the Drip Shield and Waste Package Outer Barrier.* ANL-EBS-MD-000001 REV 00 ICN 02. Las Vegas, Nevada: Bechtel SAIC Company. ACC: MOL.20010724.0082.

Byers, W.A.; Barkich, J.; Rootham M.W.; and Hundley, F. 1997. "Control of Lead-Assisted Stress Corrosion Cracking of Alloy 600 Tubing in Steam Generator Free Span Locations." *Proceedings of the Eighth International Symposium on Environmental Degradation of Materials in Nuclear Power Systems—Water Reactors, 1*, 224-231. La Grange Park, Illinois: American Nuclear Society.

CRWMS M&O (Civilian Radioactive Waste Management System Management and Operating Contractor) 2000a. *Waste Package Degradation Process Model Report.* TDR-WIS-MD-000002 REV 00 ICN 02. Las Vegas, Nevada: CRWMS M&O. ACC: MOL.20001228.0229.

CRWMS M&O 2000b. *Total System Performance Assessment for the Site Recommendation.* TDR-WIS-PA-000001 REV 00 ICN 01. Las Vegas, Nevada: CRWMS M&O. ACC: MOL.20001220.0045.

CRWMS M&O 2000c. *General Corrosion and Localized Corrosion of Waste Package Outer Barrier.* ANL-EBS-MD-000003 REV 00. Las Vegas, Nevada: CRWMS M&O. ACC: MOL.20000202.0172.

CRWMS M&O 2000d. *General Corrosion and Localized Corrosion of the Drip Shield.* ANL-EBS-MD-000004 REV 00. Las Vegas, Nevada: CRWMS M&O. ACC: MOL.20000329.1185.

CRWMS M&O 2000e. *Stress Corrosion Cracking of the Drip Shield, the Waste Package Outer Barrier, and the Stainless Steel Structural Material.* ANL-EBS-MD-000005 REV 00 ICN 01. Las Vegas, Nevada: CRWMS M&O. ACC: MOL.20001102.0340.

CRWMS M&O 2001. *Aging and Phase Stability of Waste Package Outer Barrier.* ANL-EBS-MD-000002 REV 00 ICN 01. Las Vegas, Nevada: CRWMS M&O. ACC: MOL.20010926.0007

DOE (U.S. Department of Energy) 2001a. *Yucca Mountain Science and Engineering Report.* DOE/RW-0539. Washington, D.C.: U.S. Department of Energy, Office of Civilian Radioactive Waste Management. ACC: MOL.20010524.0272.

DOE 2001b. *Yucca Mountain Preliminary Site Suitability Evaluation.* DOE/RW-0540. Washington, D.C.: U.S. Department of Energy, Office of Civilian Radioactive Waste Management. ACC: MOL.20011101.0082.

Drever, J.I. 1997. *The Geochemistry of Natural Waters, Surface and Groundwater Environments.* 3rd Edition. Upper Saddle River, New Jersey: Prentice Hall. TIC: 246732

Farmer, J.C.; Van Konynenburg, R.A.; McCright, R.D.; and Bullen, D.B. 1988. *Localized Corrosion and Stress Corrosion Cracking of Austenitic Steels.* Volume 3 of *Survey of Degradation Modes of Candidate Materials for High-Level Radioactive-Waste Disposal Containers.* UCID-21362. Livermore, California: Lawrence Livermore National Laboratory. ACC: MOL.19980715.0385.

Farmer, J.C.; McCright, R.D.; Gdowski, G.E; Wang, F.; Summers, T.S.E.; Bedrossian, P.; Horn, J.; Lian, T.; Estill, J.; Lingenfelter, A.; and Halsey, W. 2000. "General and Localized Corrosion Resistance of Outer Barrier of High-Level Waste Container in Yucca Mountain (UCRL-JC-138890, LLNL)." *Pressure Vessel and Piping Codes and Standards—2000: Proceedings of the Pressure Vessel and Piping Conference, July 23-27, 2000.* New York, New York: American Society of Mechanical Engineers.

Frost, R.R. and Griffin, R.A. 1977. "Effect of pH on Adsorption of Arsenic and Selenium from Landfill Leachate by Clay Minerals." *Soil Science Society of America Journal, 41,* 53-57. Madison, Wisconsin: Soil Science Society of America.

Hem, J.D. 1992. *Study and Interpretation of the Chemical Characteristics of Natural Water.* USGS-WSP-2254. 3rd Edition. Washington, D.C.: U.S. Geological Survey. TIC: 243429.

Hermas, A.A. 1999. "Polarisation of Low Phosphorus AISI 304 Stainless Steel in H_2SO_4 Containing Arsenite," *British Corrosion Journal, 34,* (2), 132-138. London, England: The Institute of Materials.

Hingston, F.J.; Posner, A.M.; and Quirk, J.P. 1971. "Competitive Adsorption of Negatively Charged Ligands on Oxide Surfaces." *Surface Chemistry of Oxides, Discussions of the Faraday Society, 52,* 334-351. London, England: Royal Society of Chemistry. TIC: 237679.

Kehler, B.A.; Ilevbare, G.O.; and Scully, J.R. 2001. "Crevice Corrosion Stabilization and Repassivation Behavior of Alloys 625 and 22." *Corrosion* (to be published). Houston, Texas: National Association of Corrosion Engineers.

Kim, Y.J.; Andresen, P.L.; Martiniano, P.; Chera, J.; and Larsen, M. 2001. *Passive Film Characteristics and Long Term Stability*. Interim Report NW 2001-03, August 16, 2001. Schenectady, New York: General Electric Corporate Research & Development Center.

Krabbenhoft, D.P. and Babiarz, C.L. 1992. "The Role of Groundwater Transport in Aquatic Mercury Cycling." *Water Resources Research, 28*, 3119-3128. Washington, D.C.: American Geophysical Union.

Lloyd, A.C. 2001. Student Poster Session, Corrosion/01, March 11-16, 2001. Houston, Texas: National Association of Corrosion Engineers.

MacNaughton, M.G. and James, R.O. 1974. "Adsorption of Aqueous Mercury (II) Complexes at the Oxide/Water Interface." *Journal of Colloid and Interface Science, 47,* (2), 431-440. New York, New York: Academic Press. TIC: 224554.

Maest, A.S., Pasilis, S.P., Miller, L.G., and Nordstrom, D.K. 1992. *Redox Geochemistry of Arsenic and Iron in Mono Lake California, USA, in Water-Rock Interaction.* Rotterdam, The Netherlands: A.A. Balkema.

Myneni, S.C.B.; Traina, S.J.; Logan, T.J.; and Waychunas, G.A. 1997. "Oxyanion Behavior in Alkaline Environments: Sorption and Desorption of Arsenate in Ettringite." *Environmental Science and Technology, 31*, 1761-1768. Washington, D.C.: American Chemical Society.

Oremland, R.S.; Dowdle, P.R.; Heoft, S.; Sharp, J.O.; Schaefer, J.K.; Miller, L.G.; Blum, J.S.; Smith, R.L.; Bloom, N.S.; and Wallschlaeger, D. 2000. "Bacterial Dissimilatory Reduction of Arsenate and Sulfate in Meromictic Mono Lake, California." *Geochimica et Cosmochimica Acta, 64,* 3073-3084. New York, New York: Elsevier Science.

Orme, C. 2001. "Surface Analysis of Awaruite (Josephinite) Rock, August 13, 2001." Memorandum from C. Orme (LLNL) to Tammy Summers (LLNL), August 13, 2001.

Perfect, D.L.; Faunt, C.C.; Steinkampf, W.C.; and Turner, A.K. 1995. *Hydrochemical Data Base for the Death Valley Region, California and Nevada.* Open-File Report 94-305. Denver, Colorado: U.S. Geological Survey. ACC: MOL.19940718.0001.

Pierce, M.L. and Moore, C.B. 1980. "Adsorption of Arsenite on Amorphous Iron Hydroxides from Dilute Aqueous Solutions." *Environmental Science and Technology, 14*, 214-216. Washington, D.C.: American Chemical Society.

Sano, Y.; Kimura, M.; Sato, K.; Obata, M.; Sudo, A.; Hamamoto, Y.; Shima, S.; Ichikawa, Y.; Yamazaki, H.; Naruse, M.; Hida, S.; Watanabe, T.; and Oono, Y., 2000. "Development and Application of Laser Peening System to Prevent Stress Corrosion Cracking of Reactor Core Shroud." *Proceedings of the Eighth International Conference on Nuclear Engineering (ICONE-8), ICONE-8441, Baltimore, April, 2000*. New York, New York: American Society of Mechanical Engineers.

Sano, Y.; Kimura, M.; Yoda, M.; Mukai, N.; Sato, K.; Uehara, T.; Ito, T.; Shimamura, M.; Sudo, A.; and Suezono, N. 2001. "Development of Fiber-Delivered Laser Peening System to Prevent Stress Corrosion Cracking of Reactor Components." presented at ICONE-9, the 9th International Conference on Nuclear Energy, April 8-12, 2001, Nice, France. New York, New York: American Society of Mechanical Engineers.

Stauffer, R.E. and Thompson, J.M. 1984. "Arsenic and Antimony in Geothermal Waters of Yellowstone National Park, Wyoming, USA." *Geochimica et Cosmochimica Acta, 48*, 2547-2561. New York, New York: Pergamon Press.

Swedlund, P.J. and Webster, J.G., ed. 1998. "Arsenic Removal from Geothermal Bore Waters: The Effect of Mono-Silicic Acid." In *Proceedings of the International Symposium on Water-Rock Interaction, WRI-9, Taupo, New Zealand, 30 March–3 April 1998*. Arehart, G.B. and Hulston, J.R., eds. Pages 333-336. Brookfield, Vermont: A.A. Balkema.

Tiffreau, C. and Trocellier, P. 1998. "Modelling the Sorption of Mercury (II) on (hydr)oxides: Application of Ion Beam Analysis to Sorption Processes." *Nuclear Instruments and Methods in Physics Research, B 136-138,* 308-312. Amsterdam, The Netherlands: Elsevier Science.

van der Hoek, E.E.; Bonouvrie, P.A.; and Comans R.N.J. 1994. "Sorption of As and Se on Mineral Components of Fly Ash: Relevance for Leaching Processes." *Applied Geochemistry, 9,* 403-412. London, England: Pergamon Press.

Welch, A.H.; Lico, M.S.; and Hughes, J.L. 1988. "Arsenic in Ground Water of the Western United States." *Ground Water, 26,* 333-347. Westerville, Ohio: National Ground Water Association.

Welsch, G.; Smialek, J.L.; Doychak, J.; Waldman, J.; and Jacobson, N.S. 1996. "High Temperature Oxidation and Properties." Chapter 2 of *Oxidation and Corrosion of Intermetallic Alloys.* Welsch, G. and Desai, P.D.; eds. West Lafayette, Indiana: Purdue University. TIC: 245280.

Wexler, A.S. and Seinfeld, J.H., 1991. "Second-Generation Inorganic Aerosol Model," *Atmospheric Environment, 25A*, (12), 2731-2748. Oxford, England: Pergamon Press.

Wilkie, J.A. and Hering, J.G. 1996. "Adsorption of Arsenic onto Hydrous Ferric Oxide: Effects of Adsorbate/Adsorbent Ratios and Co-occurring Solutes." *Colloids and Surfaces A: Physicochemical and Engineering Aspects, 107*, 97-110. Amsterdam, The Netherlands: Elsevier Science.

Zelewski, L.M.; Krabbenhoft, D.P.; and Armstrong, D.E. 2001. "Trace Metal Concentrations in Shallow Ground Water." *Ground Water, 39*, 485-491. Westerville, Ohio: National Ground Water Association.